Numerical simulation and population-wide risk assessment of windblown dust emission from dried-up bottom of Aral Sea

(アラル海露出海底からの砂塵巻き上げ
シミュレーションと健康リスク評価)

Bakhtiyor NAKHSHINIEV

Department of Environment Systems, School of Frontier Sciences, The University of Tokyo

Supervisor:

Professor Toru Sato

August 21, 2006

ABSTRACT

The Aral Sea, once one of the world's largest inland seas, is now shrinking due to unsustainable water consumption from its inflow rivers by the Central Asian Republics (the culprit countries - Uzbekistan, Turkmenistan, Kazakhstan, Tajikistan and Kyrgyzstan). As a consequence of the increased of irrigated area and hydropower generation in the Aral Sea basin, coupled with population increase, the Aral Sea has deteriorated into the largest inland body of salty reservoir in the world. Each year violent sandstorms pick up hundred thousands tons of salt and sand from the dried-up seabed and transport it across hundreds of kilometres. The sands are contaminated with industrial and agricultural chemicals residue and have been linked to high regional rates of respiratory diseases and certain types of cancer. A depressed fact is that the primary victims of these crises are the most vulnerable strata of the region's society, wiz children, elderly peoples with pre-existing asthmatic illness, women and less-paid inhabitants of cities and rural areas.

The main objective of this research was a simulation of dust particle transport from the exposed bottom of the Aral Sea and evaluation of annual mortality rate associated with windblown dust emission from dried bottom of Aral Sea. Study follows an integrated approach and conceptually consists of two models: (1) numerical simulation of dust concentrations blown from the dried-up bottom of Aral Sea and (2) population-wide risk assessment, which reads dust concentrations data from simulation model.

The findings from this study demonstrate that the major transport direction is S, SSW, SW and WSW, which is associated with cyclonic intrusion from northeast triggered by Siberian High (a high pressure system, which forms over Siberia). And as expected, we observed that the Aral Sea dust storm has major impact on mortality rate of the population of Uzbekistan, Kazakhstan and Turkmenistan. The number of people were affected by particle concentration in these countries, for 2003 year, have been approximated to be 1264, 143 and 107, respectively.

ACKNOWLEDGEMENTS

It is my pleasure to acknowledge my supervisor, professor Toru SATO for his guidance, advices and constant support during this study. His friendly encouragement and excellent guidance made this study more productive.

I wish to express my profound thanks to Shinichiro HIRABAYASHI, Toshio SUGITA, Semin JEON and Toshitaka OMIYA for their friendly assistance, given in various ways.

Many thanks to all my friends and colleagues for their supports in many different ways during the studies.

Bakhtiyor NAKHSHINIEV
The University of Tokyo, 2006-08-21

TABLE OF CONTENTS

1. INTRODUCTION

1.1. Statement of the Problem

The Project on Critical Environmental Zones identified the Aral Sea as one of the nine regions throughout the world in which the health and well-being of the population has been clearly declining as a result of adverse environmental changes (Johnston et al 1995).

The Aral Sea, once one of the world's largest inland seas, is now shrinking due to unsustainable water consumption from its inflow rivers by the Central Asian Republics (the 'culprit' countries - Uzbekistan, Turkmenistan, Kazakhstan, Tajikistan and Kyrgyzstan). As a consequence of the increase of irrigation and hydropower generation in the Aral Sea basin, coupled with population increase (Figure 1), the Aral Sea has been deteriorated into the largest inland body of salty reservoir in the world. Although it is termed "The Aral Sea Problem", the Aral issue includes more than what has happened to the lake itself. A large outer peripheral region around this waterbody has also been severely affected and exclusively designated as an "Ecological Disaster Zone" (Micklin and Williams, 1996). The Aral Sea case is a very prime example of how one small unsustainable action over a short period can lead to such a vast and long-term environmental disaster.

The process of degradation of the Aral Sea have not only posed environmental consequences but alongside, severe social and economic crises. Each year violent sandstorms pick up at least 500,000 tons of salts and sands from the dried-up seabed and transport it over hundreds of kilometres. According to Singer et al. (2003), salts and dusts are lifted as high as 4 km and are blown to a large adjacent area. The sands and dusts are contaminated with industrial and

agricultural chemicals residues, which have been applied to the irrigated areas along two feeder rivers (Ivanov et al., 1996) and have been linked to high regional rates of respiratory and cardiovascular diseases and certain types of cancer (Micklin, 1996; Orlovsky et al., 2001; Singer et al., 2003). However, a depressed fact is that the primary victims of these crises are the most vulnerable strata of the region's society, wiz children, elderly peoples with pre-existing asthmatic/respiratory and cardiovascular illness, women and less-paid inhabitants of cities and rural areas.

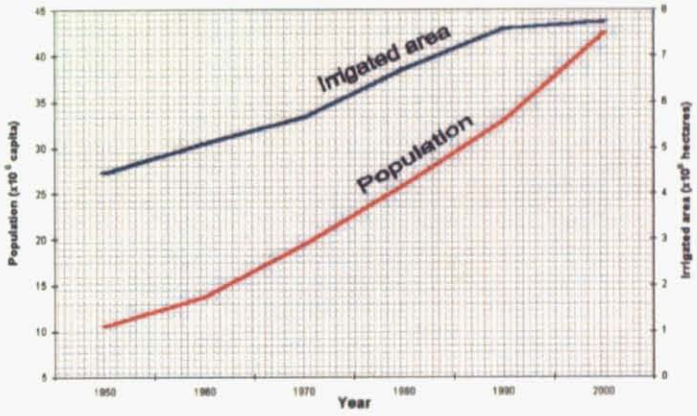

Figure.1. Synchronous increases in population and irrigated lands
(Source of data: Micklin and Williams, 1994)

1.2. Background on the Aral Sea

The Aral Sea is located in Central Asia between the Republics of Kazakhstan in the north and Uzbekistan in the south (Figure 2). It is in the centre of a large, flat desert basin. In 1960 it was the world's fourth largest lake, about 67,200 km^2 in surface area. In addition, the Aral Sea basin with a total area of 1.2 - 1.3 million km^2 covers part of the Republics of Tajikistan, Turkmenistan and Kyrgyzstan as well as northern Afghanistan. The Amu-Darya and Syr-Darya are the only influent rivers to the sea, which are heavily used for irrigation by these republics. The irrigated area extends over 28,000 km^2, and is mainly used for the cash

crops cotton and rice. This extensive irrigation is one of the major reasons why, by 1995, the volume of the Aral Sea had reduced by 75 percent. Its surface area shrank by half and the water height fell by 19 m (Figure 3). Consequently, its salinity increased more than threefold and the shoreline receded by 100 – 150 km and exposed more than 33,000 km^2 of its seabed (IFAS 2002).

Figure 2. Sketched map locating the Aral Sea

Figure 3. Chronological diminution of the Aral Sea (Adopted from FAO, 2002)

1.3. Salinisation of the sea

Salinisation is the build-up of salt within the soil, which occurs when water evaporates from the soil leaving the salt behind. In the case of the Aral Sea, as it is an endorheic lake, that is a lake without an outlet, it looses water by evaporation which gradually transformed it from being a lake into a body of salty sand reservoir. As shown in Figure 4, salinity and volume has an inverse relationship, consequently salts left behind by the receding water on increasingly large former sea bottom. This process of salinisation is one of the greatest environmental and sociological threats facing the Aral Sea region that have caused a number of adverse effects on regional flora, fauna, ecosystem and climate around the sea. But perhaps worst of all is that, the emission of this salty dust is taking death toll on public health living around the sea.

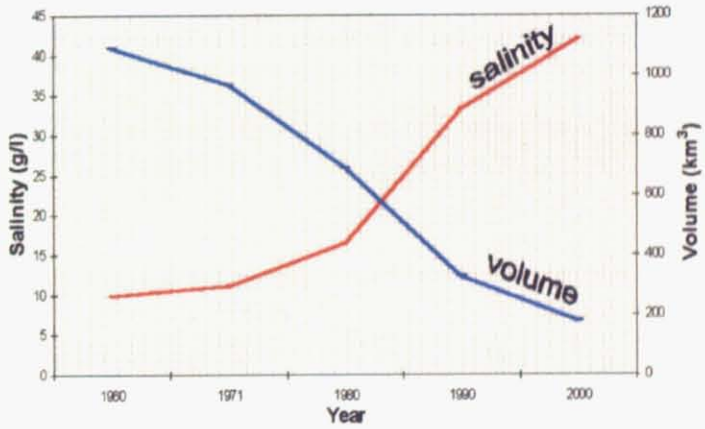

Figure 4. Trends in salinity and volume of the Aral Sea
(Source of data: Letolle and Mainquet, 1993)

1.4. Objectives

Transportation and deposition of salty dust is one of the most negative phenomena experienced at present in the Aral Sea region. The drying up of the Aral Sea has been described as one of the most staggering environmental disasters of the twentieth century. Every year, windblown dust storms originating in the exposed bottom of the Aral Sea make their way to many highly populated cities in the region. It is widely believed that this increased dust storm activity in the region has had a major impact on human health. Despite this fact, however, there is no comprehensive study on transfer of salts from the dried bottom of the sea, frequency, distribution and seasonality, estimation of its quantity and composition, the passes of transportation and those are the most important have not been investigated in great detail.

The main objective of this research is a simulation of dust particle transport and evaluation of annual mortality rate introduced by windblown dust emission from dried bottom of Aral Sea.

2. DEVELOPMENT OF WIND FLOW MODEL

2.1 Brief

The atmospheric phenomena span a huge range of scales in both space and time, and have a strong dependence on a variety of meteorological elements such as turbulence, buoyancy, topographic effect and rotation of the Earth. Understanding and predicting the regional distribution of meteorological variables (e.g. wind, pressure, temperature) of these phenomena are necessary for wind erosion simulation because they have strong relationships.

National monitoring stations are installed within the region with the purpose of providing information of ambient air pollutant concentrations and their possible impact on human health and welfare. However, although stations provide valuable information at their surrounding area, monitoring stations still leave large gap in areas where it is required to have an understanding of the concentrations. Therefore, to model the movement of dusts within the region to various vulnerable points at which it may directly be contacted by people, there was a necessity to develop the Atmospheric Wind Flow model, which can similitude the wind flow over region as accurate as possible. For this purpose an efficient computational model has been developed to simulate an unsteady three-dimensional atmospheric flow over topography with the time and spatial resolution scales of the order of kilometres and of the order of minutes, respectively. It uses as an input 6 observed or predicted atmospheric fields (Air Temperature-T, Surface Pressure-P, Sensible Heat Flux-Q, Surface Friction-u_*, Roughness Height-z_0 and Geopotential Height-Z_{GP}) and outputs three velocity components (U,V,W), pressure and air temperature for the entire calculation domain, which in turn are used as an inputs for dust particle simulation model.

2.2 General characteristics of atmospheric patterns in Central Asia

Central Asia has an extremely continental and dry climate determined by its low latitude position, its significant distance from the oceans, specific features of atmospheric circulation, and the presence of high mountain ranges in the southwest, south, and southeast. The continental climate in Central Asia is expressed by the sharp daily, seasonal, and annual variations in meteorological elements, and the high probability of dust storms. The aridity and semi-aridity of the climate is manifested by very low precipitation (100–250 mm in low attitude area and 500–650 mm in high attitude regions), low air humidity, low cloudiness, high evaporation rates (2000–2700 mm), and frequent droughts and dry winds (Orlovsky, 1994). The year in the region is specifically divided into two periods: a very dry and warm period with stable hot weather, and a relatively humid cold period with extremely unstable weather. During the cold period, Central Asia is influenced by the southwestern periphery of the Siberian High (a high pressure, which forms over Siberia, Figure 2.1) in winter and experiences air mass intrusions from the northwest and north. Cyclonic intrusions from the south, carrying tropical air, also play a significant role during the cold period: they result in unstable winter weather, increased cloudiness and precipitation, and sharp changes in air temperature and humidity. In contrast, the predominance of the Siberian High results in very severe winters with long frost periods.

During the warm period, cold invasions from the north-west and north are accompanied by strong winds, dust storms, a temperature drop of 4–6 C, and increased humidity. Significant cooling occurs rarely, and only during iterative invasions of cold air.

To sum up, during the year a successive change of air masses takes place: air masses from temperate latitudes prevail in winter, whereas continental tropical air prevails in summer.

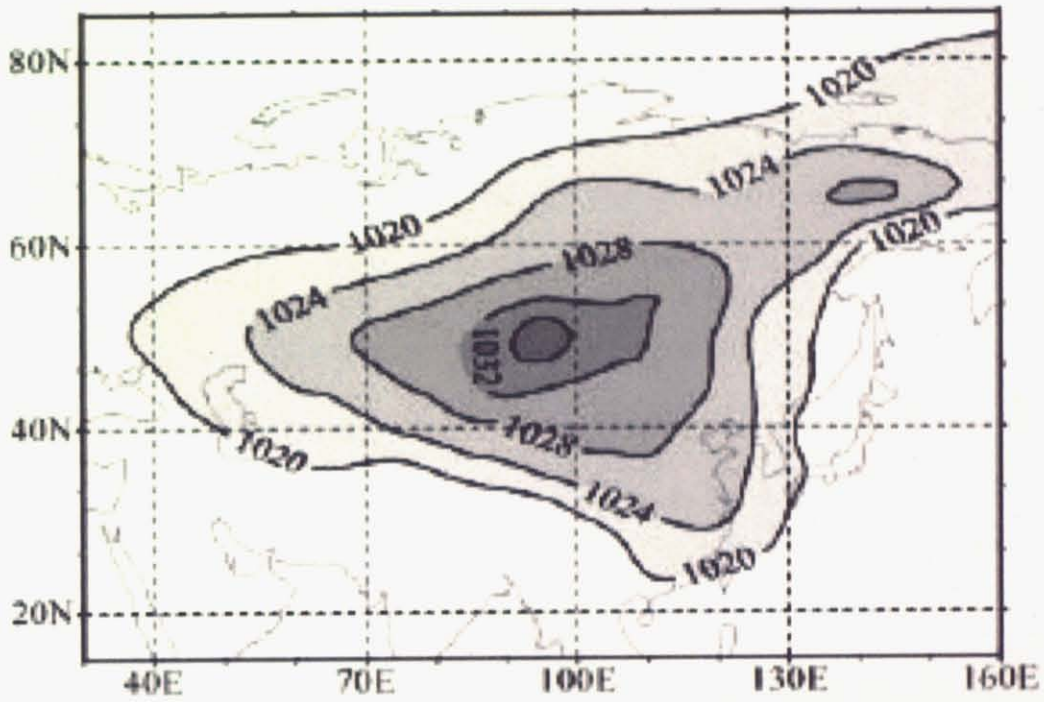

Figure 2.1 The Siberian High over the Asia continent (Source: Gong and Ho, 2002)

2.3 Sources of input data considered

Initially, three potential sources of atmospheric fields were identified for use in the study:

1. The European Centre for Medium Range Weather Forecasting (ECMWF)-output from an on-going reanalysis of atmospheric data.
2. National Centre for Atmospheric Research (NCAR)-6-hourly (recorded at 00:00, 06:00, 12:00, 18:00) data, gridded at a resolution of 2.5° latitude by 2.5° longitude.
3. UK Meteorological Office-daily/monthly mean atmospheric data for the Northern Hemisphere.

Of these data sources, the NCAR data set was considered to be the best record of atmospheric data available (Yang, 2006, personal communication).

2.4 Grid system

The most important factor to the success of the simulation of the atmospheric flow over three-dimensional topography is how to specify the topography model as a boundary condition in the computation. For this purpose we used the grid system (Figure 2.1, a,b,c), with terrain-fitted coordinate system. It follows the smooth function and with higher density of layers near the terrain. This technique is used to discretize the whole air domain.

The model consists of 143 and 110 grids in horizontal direction with resolution of 15 km and 30 layers in vertical direction with 4 m height in lowest layer and up to 2000 m in upper layer.

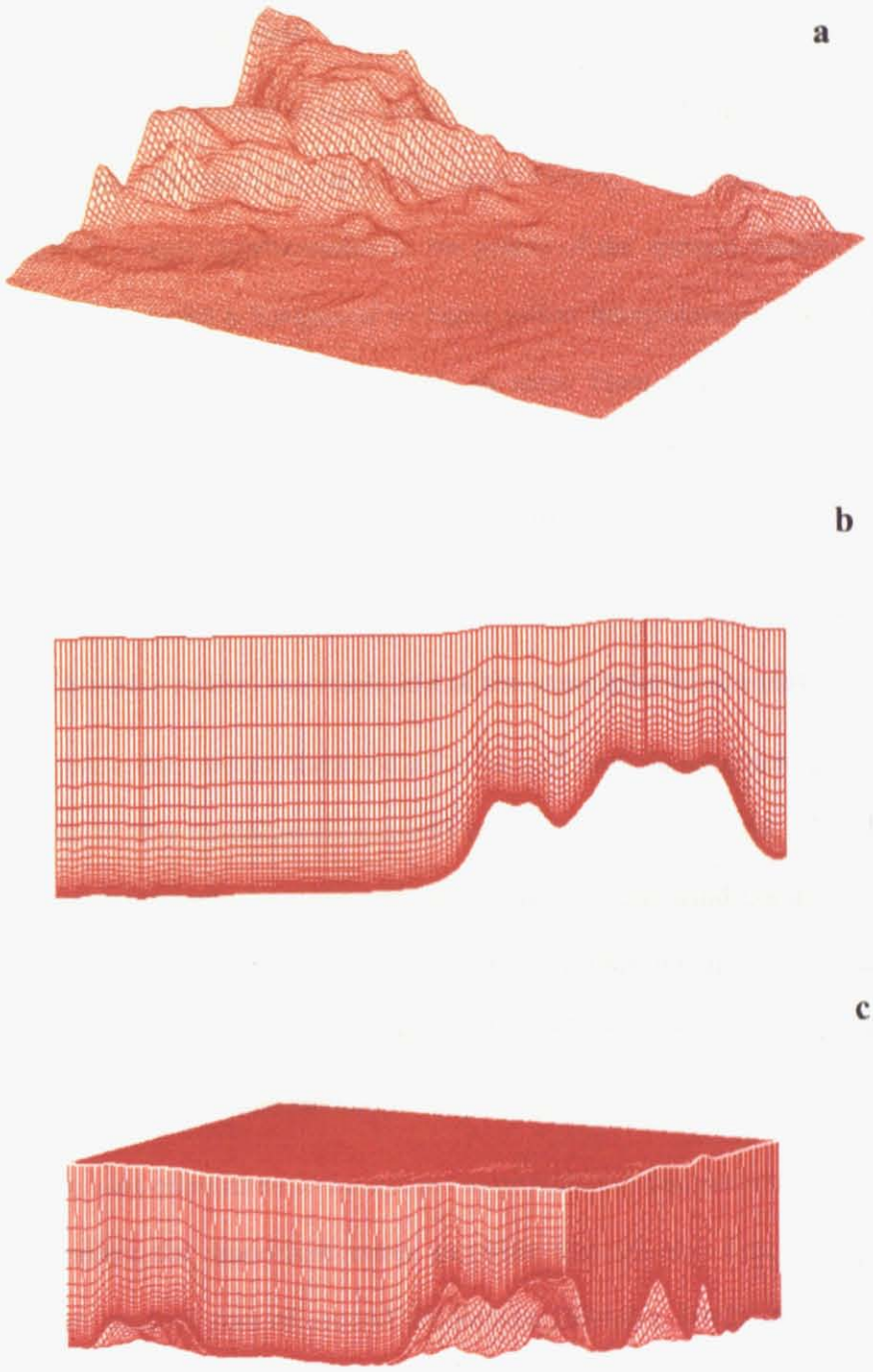

Figure 2.2 The grid system: a) digitilized topography of the region b) XZ-cross-section, and c) dicretised air domain (factor size ratio X=1, Y=2 and Z=80).

2.5 Wind field computations process

Initially, the wind filed was obtained in two steps. First, the values of Surface Friction-u_*, Air Temperature-T, Surface Pressure-P, Sensible Heat Flux-Q, Roughness Height-z_0 and Geopotential Height-Z_{GP} were approximated in the points of the domain located at the same height z_0 over the terrain using a *horizontal bi-cubic spline interpolation*. The z_0 here is the height at which the wind speed normally equals to zero. Then from this information we perform a *vertical extrapolation* to define the velocity filed in the whole domain. To find the fields at desired time, temporary interpolation was also carried out.

2.5.1 Horizontal (*bi-cubic spline*) interpolation of the atmospheric elements

The NCAR atmospheric data are available on a 2.5° x 2.5° latitude/longitude grid. However, the atmospheric data in this model were required on 15 km x 15 km grid. Therefore, these data had to be interpolated onto the finer grid for performing the wind computations. Since the key meteorological elements are relatively smooth varying fields, bi-cubic spline interpolation techniques were used that give smoothly varying estimates that are accurate at the grid points. The algorithm of this method is fully described by Press et al. (1992).

A variant of bi-cubic uses one-dimensional splines to provide the derivatives information. The bi-cubic spline provides the smoothest curve possible through the data, in the sense of minimising the mean squared sum of second derivatives (Watson, 1992). A disadvantage of this method is that in regions of high gradient and sharp changes in direction of raw data, the interpolation can fail giving unusual negative or extremely high value of variables such as roughness height. However, the surface roughness height data for the region in this study are likely not to suffer so much from sharp changes in direction. Only for the very few original

grid points, especially near the mountains, which slope at a high angle, these sharp increases were found. To control this problem and allow realistic interpolation evidence of overrunning were searched and reduced to the more acceptable value.

2.5.2 Vertical extrapolation

In this study, a log-linear wind profile is considered in vertical direction. This takes into account the horizontally interpolated variables and the effect of roughness on the wind intensity and direction (Montero, 1998). These values also depend on the air stability (neutral, stable or unstable atmosphere). Above the surface layer (Z_{sl}), a linear interpolation is made using the geostrophic wind. The logarithmic profile of wind in vertical direction is given by

$$u(z)=\frac{u_*}{k}\left(\log\frac{z}{z_0}-\psi_m(\frac{z}{L})\right). \qquad (2.5.1)$$

Where u_* is friction velocity, k-is Von-Karman constant, z_0- is the roughness height and Z_{sl} is the height of the surface layer. The value ψ_m depends on the air stability and obtained by following equations (Stull,1988).

For neutral atmosphere, $\frac{z}{L}=0$,

$$\psi(\frac{z}{L})=0, \qquad (2.5.2)$$

for stable atmosphere, $\frac{z}{L}>0$,

$$\psi(\frac{z}{L})=-5*\frac{z}{L}, \qquad (2.5.2)$$

and finally for unstable atmosphere, $\frac{z}{L} < 0$,

$$\psi(\frac{z}{L}) = \log\left[\left(\frac{x^2+1}{2}\right)\left(\frac{x+1}{2}\right)^2\right] - 2\arctan x + \frac{\pi}{2} \qquad (2.5.3)$$

where, $x = (1-16z/L)^{1/4}$ and L is Obukhov Length.

The Obukhov Length is given by (Stull,1988):

$$L = \frac{u_*^2 T}{kg\theta_*} \qquad (2.5.4)$$

where u_* is friction velocity, T-absolute temperature in Kelvin, k=0.42, Karman constant, g-is gravity and θ_* is the temperature scale or just the friction temperature.

Friction temperature is calculated by:

$$\theta_* = -\frac{Q}{\rho_{air} C_p u_*} \qquad (2.5.5)$$

where u_* is friction velocity in m/s, C_p=*1004.9,* specific heat of moist air at sea level in $m^2 s^{-2} K^{-1}$, ρ_{air} is air density in kg/m^3, and Q is sensible heat flux in *Km/s.*

The height of the boundary layer (h_{BDL}) above the ground is chosen such that the wind intensity and direction is the same for all the layers at that height (Georgieva, 2002).

For neutral condition, $\mu = 0$,

$$h_{BDL} = 0.3\frac{u_*}{f_c}, \qquad (2.5.6)$$

for stable condition (Zilitinkevich, 1989), $\mu > 0$,

$$h_{BDL} = 0.3\frac{u_*}{f_c}\frac{1}{(1+0.882\sqrt{\mu})}, \tag{2.5.7}$$

for unstable condition (Ratto et al., 1990), $\mu < 0$,

$$h_{BDL} = 0.3\frac{u_*}{f_c}(1+1.581\sqrt{-\mu}), \tag{2.5.8}$$

where μ is stability parameter and defined by (Georgieva, 2002)

$$\mu = \frac{ku_*}{f_c L} \tag{2.5.9}$$

Then the height of surface layer is defined by (Georgieva, 2002)

$$h_{surf} = h_{BDL}/10. \tag{2.5.10}$$

To maintain the generality of smooth change in wind direction above the surface layer, a linear interpolation with geostrophic wind V_g is done as follows (Montero,1998):

$$u_0(z) = \rho(z)u_0(z_{sl}) + [1-\rho(z)]U_G, \quad z_{sl} \le z \le h, \tag{2.5.11}$$

Where $\rho(z)$ is,

$$\rho(z) = 1-\left(\frac{z-z_{sl}}{h-z_{sl}}\right)^2\left(3-2\frac{z-z_{sl}}{h-z_{sl}}\right). \tag{2.5.12}$$

For one example grid point (I=122, J=49), figure 2.3 shows the increase in wind speed and change in its direction with height, between surface and 685 m (K=18). These changes are in accordance with (2.5.12).

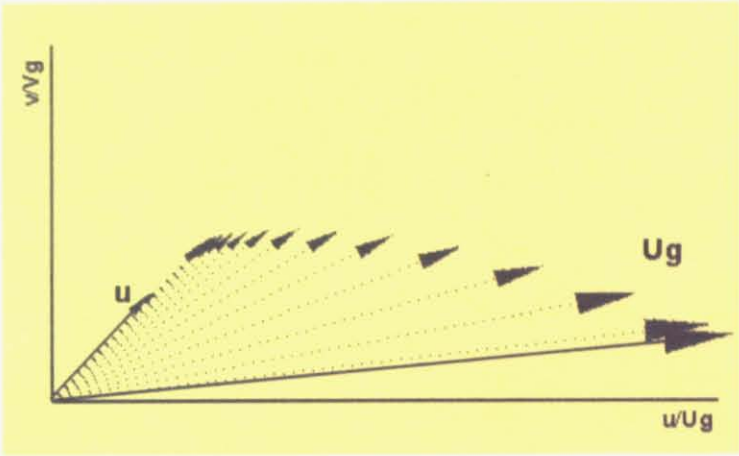

Figure 2.3 Turning wind with the height

Finally, this model assumes that $u(z)=U_g$ if z> h, and $v(z)=0$, *if* $z<=Z_0$. Bellow Figure 2.4 shows a typical vertical profile of wind velocities, which represents Equations (2.5.1) and (2.5.12), and the last two assumptions, in the stratified boundary layer.

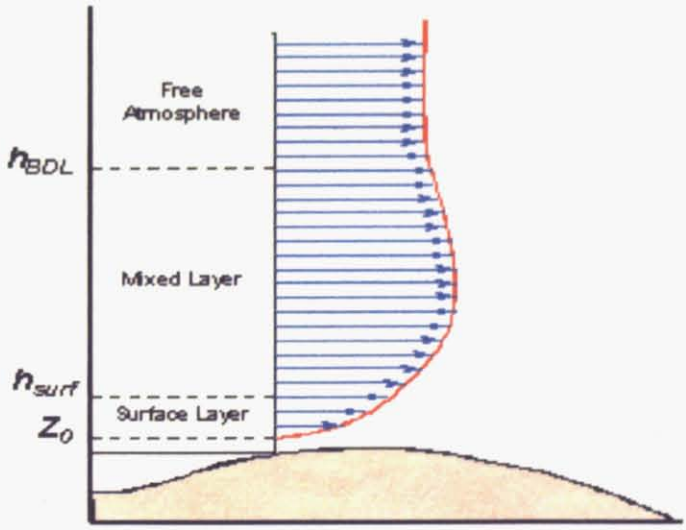

Figure 2.4 An illustrative example of a vertical profile of wind. Boundary layer stratification

2.6 Vertical wind velocity.

The vertical wind velocity is not an observed variable, and yet, its estimation appears as one of the most difficult problem for the meteorologists. However, if the wind observation is available on a grid array, the estimation of kinematic vertical velocity can obtained straightforwardly from the integration of the mass continuity equation.

The equation of continuity is:

$$\frac{\partial u}{\partial x}+\frac{\partial v}{\partial y}+\frac{\partial w}{\partial z}=0 \qquad (2.6.1)$$

Under this strong constrain of mass conservation the vertical motion is obtained by:

$$w(z)=-\int_0^z\left(\frac{\partial u}{\partial x}+\frac{\partial v}{\partial y}\right)dz. \qquad (2.6.2)$$

2.7 Horizontal eddy diffusivity.

The Richardson theory has been used to estimate horizontal eddy diffusivity in the present research. The Richardson theory is

$$K_H = D = \alpha * l^{4/3} \qquad (2.7.1)$$

where α is constant and assumed 10^{-6}, and l represents the horizontal grid length in *cm*.

2.8 Parameterisation of the vertical eddy diffusivity.

The eddy diffusivity is best not kept constant (Stull, 1988). The expression of eddy diffusivity for surface layer used in this study is same as proposed set of equations by Stull, (1988),

$$K_Z = \frac{kzu_*}{\phi_M(z/L)}. \qquad (2.8.1)$$

where L the Obukhov length given by (2.5.4) and $\phi_M(z/L)$ is dimensionless shear depending on atmospheric stability and approximated by

$$\phi_M(z/L) = \begin{cases} 1 + (4.7\frac{z}{L}) & for\ \frac{z}{L} > 0\ (stable\ ) \\ 1 & for\ \frac{z}{L} = 0\ (neutral\ ). \\ \left[1 - (\frac{15z}{L})\right]^{-1/4} & for\ \frac{z}{L} < 0\ (unstable\ ) \end{cases} \qquad (2.8.2)$$

Above the surface layer, a linear interpolation with $K_{Tropo.}$ $(=1m^2/s)$, troposphere eddy diffusivity is conducted as follow:

$$K_Z = \rho(z)K_Z(z_{sl}) + [1-\rho(z)]K_{Tropo.}, \quad z_{sl} \le z \le h, \qquad (2.8.3)$$

where $\rho(z)$ is obtained by expression of (2.5.12).

2.9 Geostrophic wind calculation.

Geostrophic wind is wind basically calculated from surface pressure data. A balance is assumed between the flow of air from high to low pressure regions and the effects of the rotation of the Earth. It is a good approximation to the actual wind in the free atmosphere (Watson et al., 1998).

The geostrophic wind is the horizontal equilibrium wind (V_G), blowing parallel to the isobars, which represents the balance between the horizontal pressure gradients force (James, 1994):

$$F_p = -\left(\frac{1}{\rho}\right)\nabla_H p \qquad (2.9.1)$$

and the horizontal component of the Coriolis Force:

$$F_c = fV_G \tag{2.9.2}$$

where $\nabla_H p$ is the horizontal pressure gradient, ρ is the air density, and f is the Coriolis parameter, which is a function of the Earth's angular momentum(Ω) and latitude (φ):

$$f = 2\Omega\sin\varphi. \tag{2.9.3}$$

The magnitude of V_G is given by

$$V_G = \left|\left(\frac{1}{f\rho}\right)\nabla_H p\right|. \tag{2.9.4}$$

The geostrophic wind speed is a function of latitude, pressure gradient and air density, a quantity that is not measured routinely. However, there are equivalent ways of presenting the same information. Holton (2004) related high-pressure areas to high heights, and low-pressure areas to low heights of a constant pressure surface. And geostrophic wind was expressed in more suitable form, which has the advantage that it does not include the air density. Geostrophic wind using geostrophic balance can be writing as

$$-g\frac{\partial Z}{\partial N} = fV_G \tag{2.9.5}$$

and, hence

$$V_G = -\frac{g}{f}\frac{\partial Z}{\partial N} \tag{2.9.6}$$

In performing a calculation, $\partial Z/\partial N$ is approximated by $\Delta Z/\Delta N$ where ΔZ is the height interval between adjacent contour lines, and ΔN geographical distance between contour lines and measured perpendicularly between the lines.

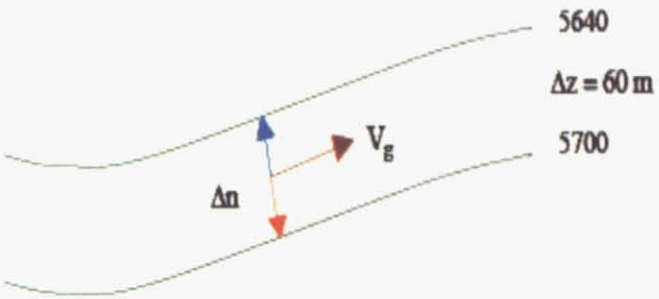

Figure 2.5 An illustrative example of a geostrophic wind calculation

Figure 2.6 illustrates the calculated geostrophic wind vectors and the contours of geopotential heights for a stormy day, April 18, 2003. In Figure 2.7 the stream function from geopotential height is drawn for the same day. The wind vectors well paralleled to contour lines allow us to judge that approximation is accurate enough to represent the geostrophic wind over the region.

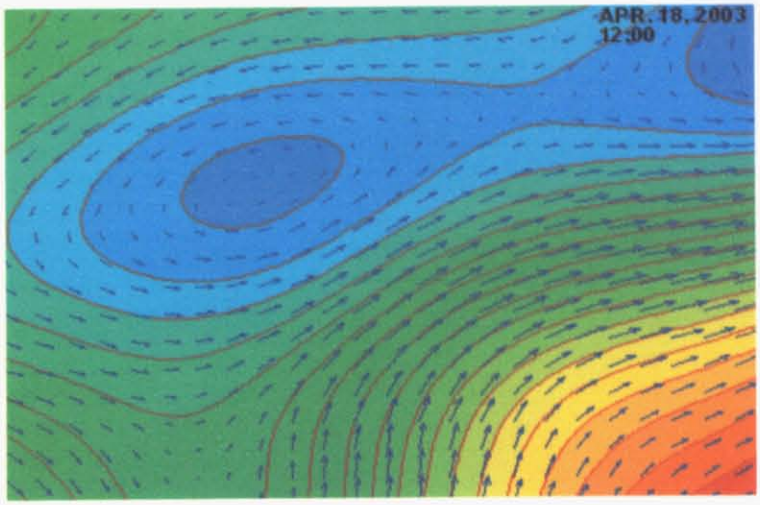

Figure 2.6 The contours of geopotential height and calculated geostrophic wind vectors

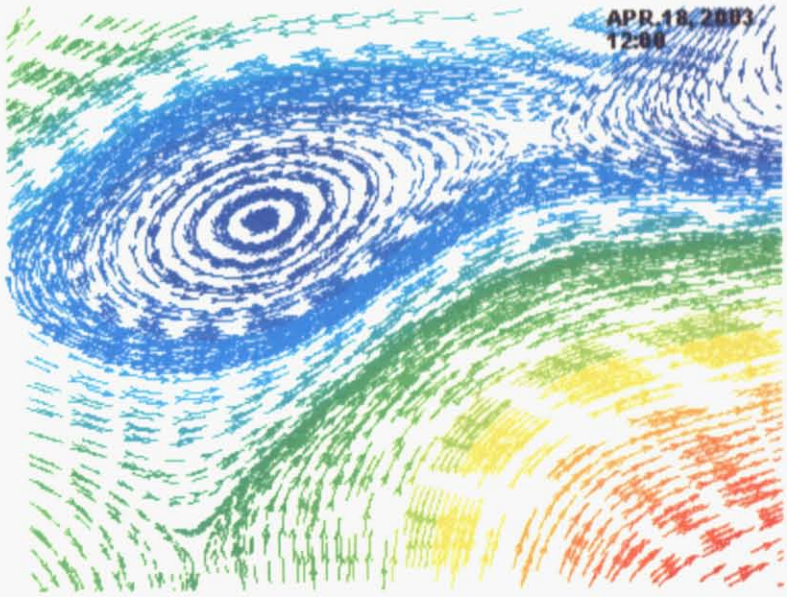

Figure 2.7 Stream function from interpolated geopotential heights

2.10 Temporal Interpolation

Temporal linear interpolation is done following relation:

$$V_{now} = V_0 \frac{t_6 - t_{now}}{t_6 - t_0} + V_6 \frac{t_{now} - t_0}{t_6 - t_0} \qquad (2.10.1)$$

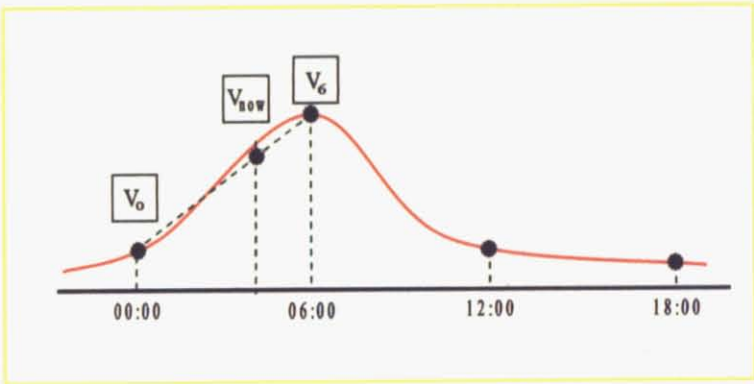

Figure 2.8 A graphical demonstration of temporar interpolation

The results of 1-hourly temporary interpolated surface temperature for the day of April 1, 2003, is demonstrated in Figure 2.9.

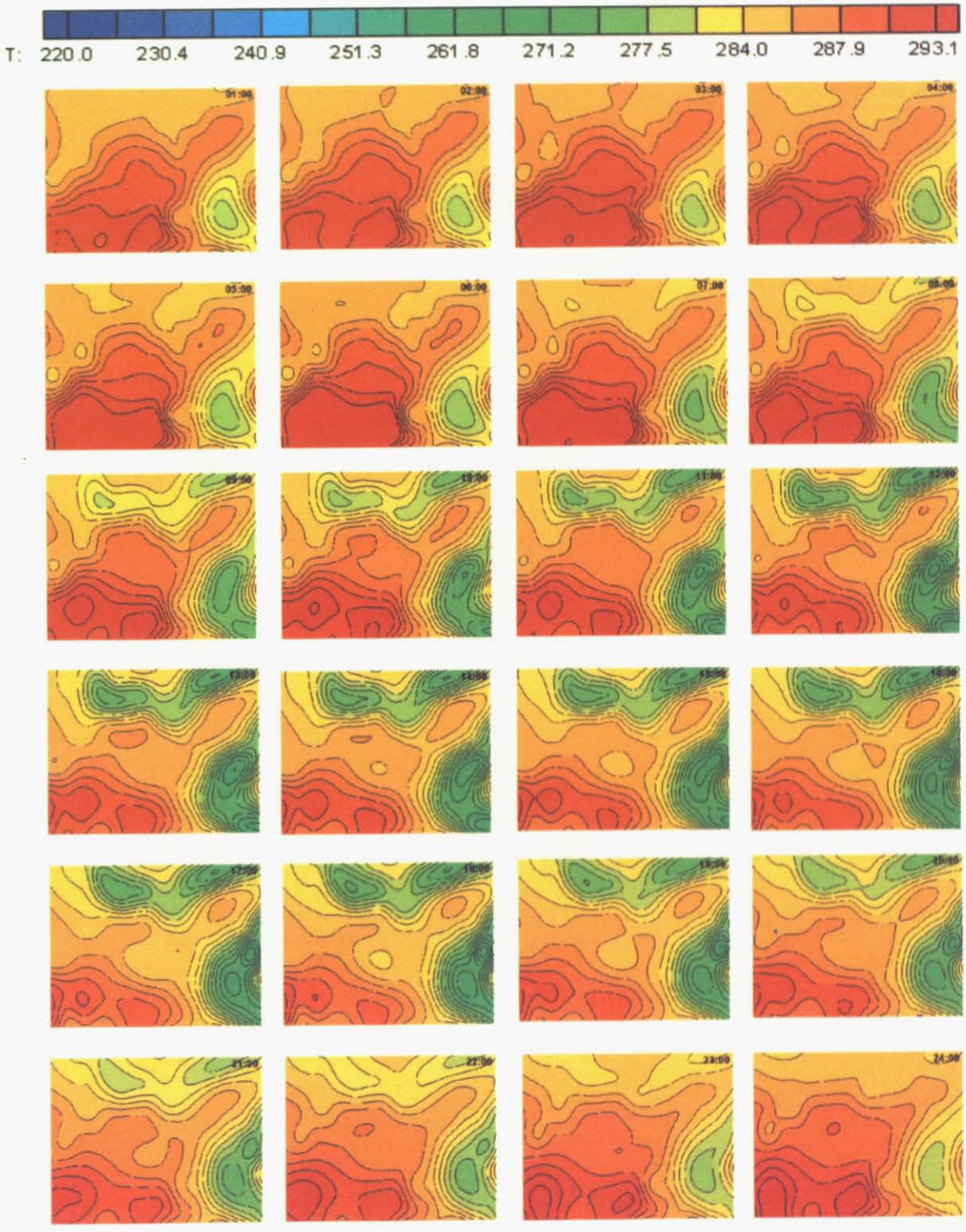

Figure 2.10 Plots of temporary interpolated surface temperature

2.11 Methods of comparison

In order to test the efficiancy of the model, two methods of comparisiton were considered. First, contour map of U and V wind components at 10 meter, calculated from interpolated friction velocity, are compared with the contour map of standard 10-meter wind field from NCAR ongoing reanalysis model. Differences between the charts will be described where relevant. The contours are drawn on-line by GrADS software. Therefore, there was no user-set option for drawing the wind vectors. Next, the daily average near ground (10-meter) wind velocities, at 5 points, compared to measured 10-meter wind field from archived NCAR data set. The points are choosen here, are located in the most populated cities, Ashkhabad, Almaty, Bishkek, Dushanbe and Tashkent.

2.11.1 Comparison of contours

In stormy day there are many closely packed contour lines thus providing the best case then ever to evaluate the model results. One stormy day, April 18, 2003, was chosen, for each meteorological chart at 00:00, 06:00, 12:00 and 18:00 local standard time.

This was the storm that triggered by Siberian High; cold air intrusion (Figure 2.12) followed by strong southwest winds (Figure 2.13) and devastated much of north and northwest part of the region. In Figure 2.11 a comparison of contour map of the near the ground (10 m) wind components (U, V), computed from interpolated friction velocity, are demonstrated versus reanalysed wind data from NCAR. As can be seen, there is very little difference. And the reason for this difference is that the most storms are very unusual event with the extremely high gradients over the short distance and the dependency of wind intensity on local stability is almost insignificant. Fortunately, the storm is very rare phenomena in the atmosphere. Therefore, in general, the model can provide a better match with the observed data.

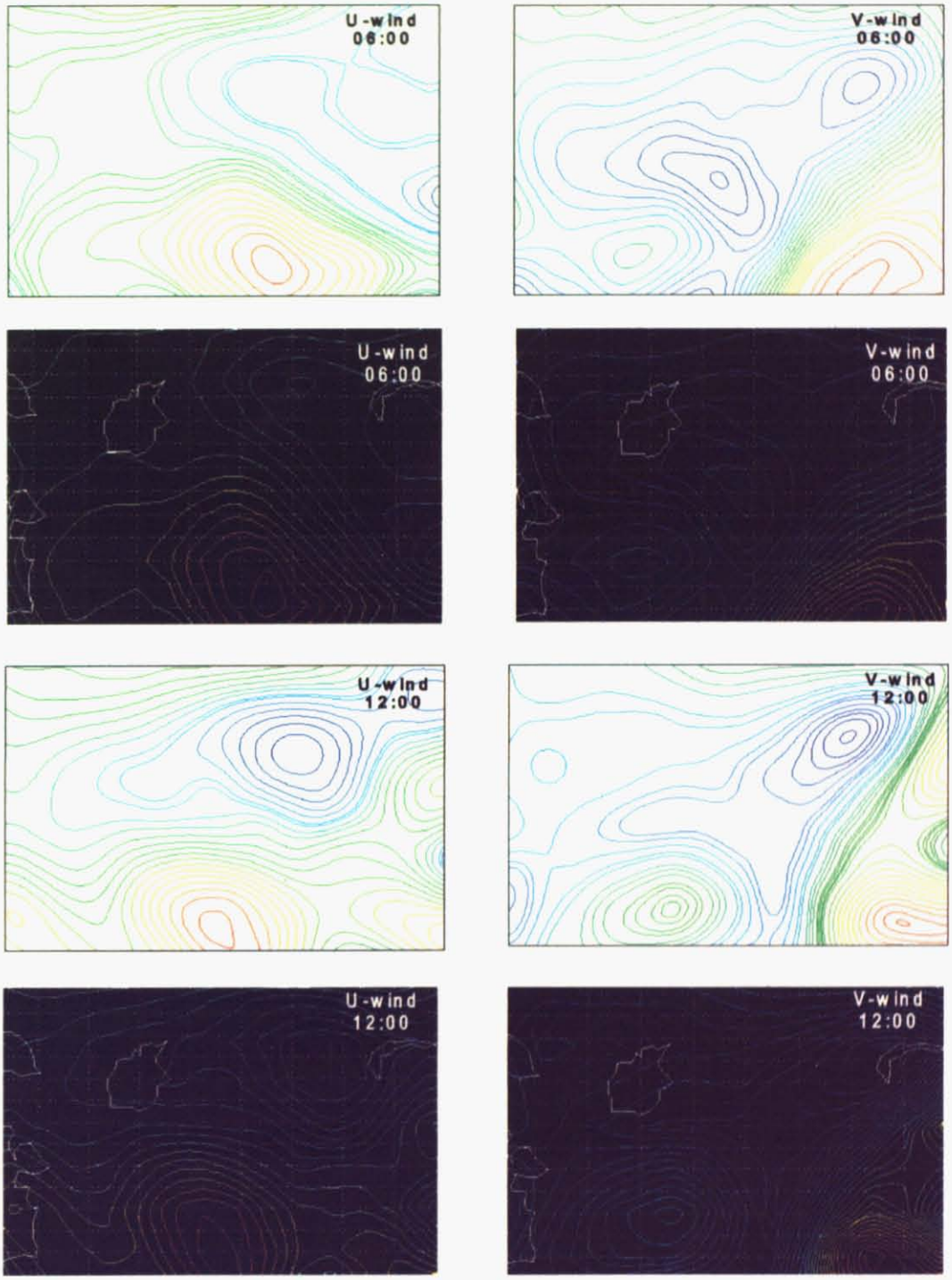

Figure 2.11 Plots of U and V wind contours at 06:00 and 12:00 local time
(The plots with the white background is the wind calculated from the interpolated friction velocity, and the one with the black background is drawn on-line from observed and reanalysed 10-meter wind data).

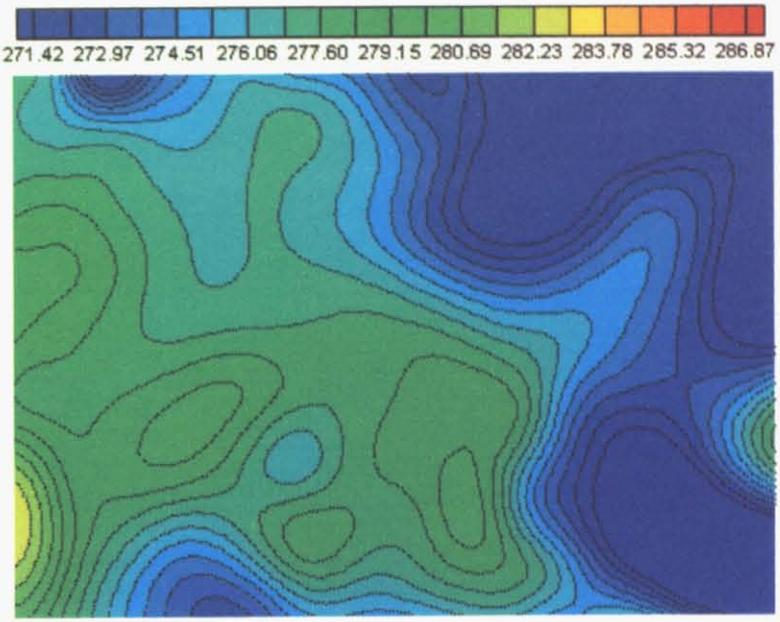

Figure 2.12 Coutours of air temperature

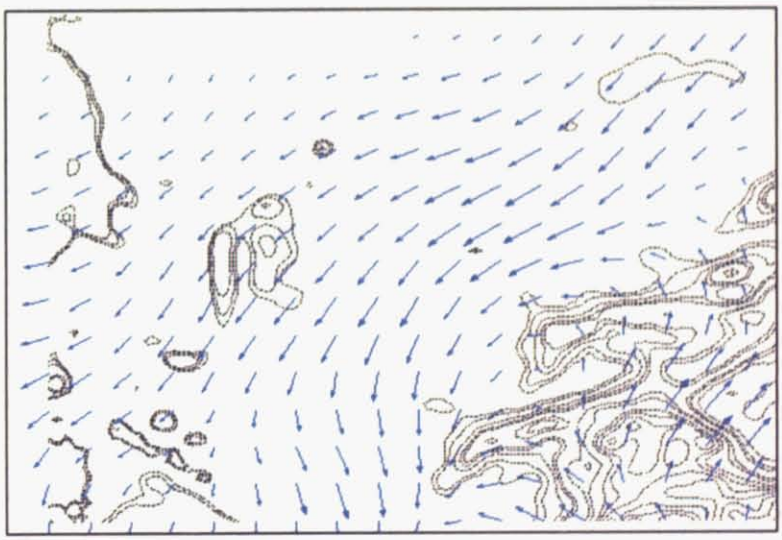

Figure 2.13 Wind field vector at 12:00 local time, Arill 18, 2003.

2.11.2 Comparison with measurements

In this section, daily averaged grid results are compared with corresponding daily averaged wind velocity from measurements at seven sites. Comparison is done for one computational year starting from January 1, 2003 ending December 31, 2003. The location of these sites is marked in Figure 2.14.

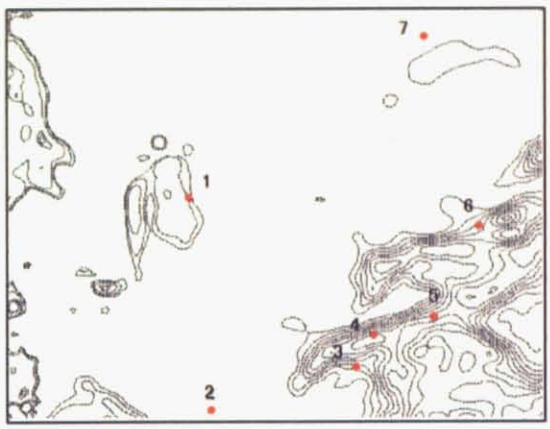

Figure 2.14 Map indicating the aproximate position of the sites.

Figure 2.15 demonstrates the comparison of daily averaged wind velocity from measurement and model results. The calculated flow pattern at all sites is similar to observed. As can be seen from figure, both measured (red) and modelled (blue) vectors are well overlapped and thus are of the same order of magnitude. The significant differences in wind speed and direction are revealed at site 7. This overestimation of wind speed by model should be expected from interpolation routine, introduced by interpolated friction velocity and sensible heat flux. A very small error in these two elements can lead to considerable over or underestimation of wind intensity and direction. In general, it is worthy of notice that the calculated and measured winds are in good agreement from both qualitatively and quantitatively point of view.

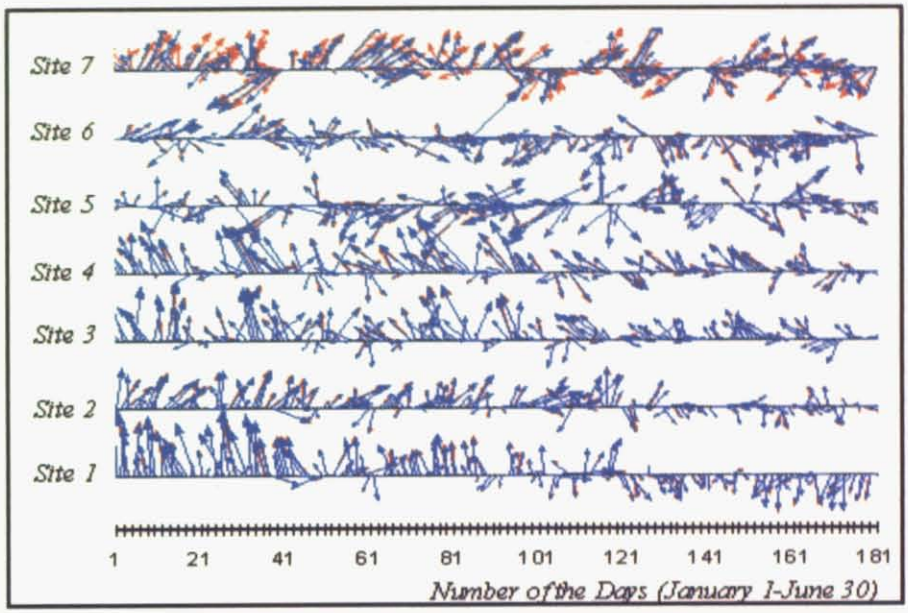

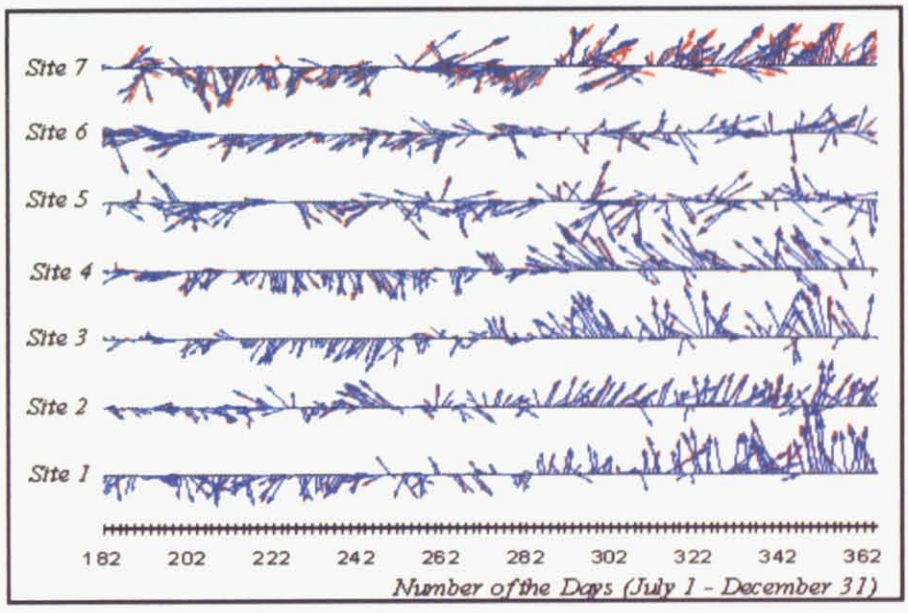

Figure 2.15 Wind field comparison at selected sites.
(The red collared vectors indicate daily averaged wind from mesurment, and the blue vectors represent modeled daily average at 10 meter above ground)

3. MODELLING OF DUST TRANSPORT

3.1 Preface

Transportation and deposition of salty dust is one of the most negative phenomena experienced at present in the Aral Sea region. The drying up of the Aral Sea has been described as one of the most staggering environmental disasters of the twentieth century. Over the last 40 years over 40 000 km^2 of the former seabed have been exposed, creating a potentially significant salty dust source. It is widely believed that this increased dust storm activity in the region has had a major impact on human health. Despite this fact, however, there is no comprehensive study on transfer of salts from the dried bottom of the sea, frequency, distribution and seasonality, estimation of its quantity and composition, the passes of transportation and those are the most important have not been investigated in great detail. Several excellent reports and papers have already been published about the problem, for instance by Razokov and Kosnazarov (1996), Denisov (1998), Kamolov (1998), Semenov (1998), Tolkacheva et al. (1998), Chernyshev (1998), Esenov (1998), Orlovsky (2004). However, the results presented in these published papers appear to be mainly experimental and lacking in documentation of the computational modelling techniques. Thus this research, particularly this chapter, is considered to go some way towards bridging this gap.

This chapter devoted to the description and formulation of transport and deposition modelling of sand and dust particles. The number of findings, dust storm patterns and its major pathways, detected by the model, compared with satellite image. It also provides input data for the next submodel, which evaluates the contribution of dust, blown from the former Aral Sea seabed, on national Standardized Death Rate for respiratory diseases.

3.2 The Morphological Features of the Soil of Dried Bottom of the Sea

The decrease of the sea level has led to a change in the *halogeochemical* process. Before the level decrease, the Aral Sea was a receiver of salts about 23.8 m tonnes of salts per year, came into the sea with the surface flow, and about the same volume with the underground flow (Chernenko, 1986). At present the drying seabed is playing a role of deliverer of salts for transportation to other regions, because the exposed bottom of the sea represents a giant salty surface. By their morphological features the soils of the dried bottom are crusty and puffy *solonchak*. By chemical composition the soil is *sulfate-chloride* and *chloride-sulfate*, formed on the sandy and sandy loamy maritime soils (Singer et al., 2002). By salt content the soils are heavy salinized soils with 50-60% and more of *sulfate* and *chloride* salts. Predominance of the soils with light texture favours the development of wind erosion processes and formation of aeolian forms of relief. Intense salt accumulation and aeolian transformation of the dried bottom of the Aral Sea led to the formation of a powerful site of salt and dust transportation source.

3.3 Annual Average Salt/Dust Removal

The assessment of the volume of salt-dust transfers from the dried bottom of the Aral Sea and its composition, the directions of its transportation and areas of deposition became of significant public and scientific concern as soon as water level in it began to drop. This interest is created because of the negative influence of salt storms on the environment and as well as living conditions of the region's population. Estimations by different researchers of the volume of salt and dust removal from the dried bottom of the Aral Sea are very contradictory. The most reliable and recent data on the amount of salt and dust removal from the dried bottom of sea was obtained by Kazakh researchers: Galaev and Semenov (1997). Based on field measurements on the rate of flow of solid particles and wind speed in the

near-ground layer during the dust storms and laboratory measurements, they have assessed the annual average of aerosol removal to be 690 000 tonnes per total exposed area.

3.4 Brief Description of the Scheme

The ambient dust concentration, which is required for the study air quality and public health assessment, should be estimated adequately. The distance dust particle travel depends on the prevailing atmospheric conditions and the emission processes from the source, which are extremely complex to model. For the specific research objective and atmospheric condition, it is useful to set up relationship between field measurements data and transport model, rather than using simple, crude and unpredictable schemes. As an approach to the solution of this problem, in the present study, particle emission rate is estimated from the annual average of particle removal, 690 000 t /yr (or 21,88 kg/exposed area/s) (Galaev and Semenov, 1997) from the exposed sea bottom. For the particle motion simulations a Lagrangian approach is used. In this formulation each computational particle is thought to represent a group of particles possessing the same characteristics such as size, composition, etc. The total N-particles number, which is realised from the source at each time step, is assumed to represent the surface vertical dust flux (or 21,88 kg/exposed area/s) emitted at given time step. In this model only dry gravitational deposition is considered. Although knowing that the wet removal is important process a large uncertainty exists in available wet removal schemes. Because of the nature of this problem and limitation of present system the wet deposition is not taken into account.

3.5 Particle Size Considered

From the perspective of air quality, the concentration of small particles is of concern to human health and thus the concentration of particles smaller than $20\mu m$ is an important indicator of air quality. For the purpose of findings the major dust storm patterns the upper

limit of particle size is set to 100 micron in diameter. During the computation of particle motion the particles sizes are chosen randomly from Gaussian probability distribution function with 50-micron mean and standard deviation 60 and 10 respectively.

3.6 Formulation of Transport Model

The transport scheme predicts the dust concentration by solving the following system of equation in Lagrangian framework:

$$\underbrace{\left(m_p + \frac{\rho_f V_p}{2}\right)}_{I}\underbrace{\frac{d\mathbf{u}_p}{dt}}_{II} = \underbrace{-V_p \nabla P}_{III} + \underbrace{m_p \mathbf{g}}_{IV} - \underbrace{\frac{1}{2}\rho_f S C_D \mathbf{u}_r |\mathbf{u}_r|}_{V} \tag{3.6.1}$$

$$\frac{d\mathbf{x}_p}{dt} = \mathbf{u}_p \tag{3.6.2}$$

Term I *describes particle mass and added mass.*

Term II *represent storage of mean particle momentum.*

Term III *describes pressure-gradient force.*

Term IV *allows gravity to act in the vertical direction only.*

Term V *is aerodynamic forces on a particle.*

Here $\mathbf{x}_p$ is the particle position, m_p is the particle mass, ρ_f is the fluid (air) density, V_p is the volume of particle, $\mathbf{u}_p$ is the particle velocity, ∇P is the pressure gradient, $\mathbf{g}$ is gravity, S is the cross-section of the particle in $\mathbf{u}_r$ direction, C_D is the drag coefficient, $\mathbf{u}_r$ is particle-to-fluid relative velocity, which is defined by

$$\mathbf{u}_r = \mathbf{u}_p - \mathbf{u} \tag{3.6.3}$$

The value of $\mathbf{u}$ is determined by interpolating fluid velocity from grid point to the location of particle.

The effect of the subgrid turbulent fluctuations of air motion are also need to be considered in the calculation of particle motion, therefore, x_p is expressed as

$$\mathbf{x}_p^{n+1} = \mathbf{x}_p^n + \Delta t \mathbf{u}_\mathbf{p} + \sqrt{2K_p \Delta t}\chi \tag{3.6.4}$$

where the last term in the equation represents a simple dispersion of particles, adopted from Suzuki (2001). K_p, here, expresses particle eddy diffusivity and χ represents the Gaussian probability distribution function. The numerical solution of this function described in Press et al. (1992).

The magnitude of the aerodynamic drag ($C_D(Re_p)$) depends on the flow patters around the particle. The $C_D(Re_p)$ relationship has been approximately determined by using Morci and Alexaner (1972) functions

$$C_D(Re_p) = \frac{k_1}{Re_p} + \frac{k_2}{Re_p} + k_3 \tag{3.6.5}$$

for different regimes of Re_p, in the form

$$C_D = \begin{cases} 24/Re_p & Re_p \le 0.1 \\ 22.73/Re_p + 0.0903/Re_p^2 + 3.69 & 0.1 < Re_p \le 1 \\ 29.1667/Re_p - 3.8889/Re_p^2 + 1.222 & 1 < Re_p \le 10 \\ 46.5/Re_p - 116.67/Re_p^2 + 0.6167 & 10 < Re_p \le 100 \\ 98.33/Re_p - 2778/Re_p^2 + 0.3644 & 100 < Re_p \le 1000 \\ 148.62/Re_p - 47500/Re_p^2 + 0.357 & 1000 < Re_p \le 5000 \\ -490.546/Re_p + 578700/Re_p^2 + 0.46 & 5000 < Re_p \le 10000 \\ -1662.5/Re_p + 5416700/Re_p^2 + 0.5191 & 10000 < Re_p \le 50000 \\ 0.48802 & 50000 < Re_p \end{cases} \tag{3.6.6}$$

The particle Reynolds number defined as

$$Re_p = \frac{|\mathbf{u}_p - \mathbf{u}| D_p}{\nu_{air}} \tag{3.6.7}$$

where ν_{air} air viscosity and D_p is particle diameter.

In this model all particles are assumed to have spherical shape, thus the volume of particle was calculated by

$$V_p = \frac{1}{6}\pi D^3 \tag{3.6.8}$$

and cross-section of particle using

$$S = \pi D^2 / 4 \tag{3.6.9}$$

-

3.7 Eddy Diffusivity of Particle

Dust particles in the atmosphere are heavy particles, as their density (around 1600 kg/m^3) is much lager than of the air (around 1.22 kg/m^3). When compared with air parcels, dust particles have different response characteristics to change in the airflow field. As a consequence dust particle and air parcels follow different trajectories during turbulent diffusion (Shao, 2000). It is therefore to be expected that the eddy diffusivity for particles differ from that for air parcels. Shao (2000) based on Csanady's (1963) theory described particle eddy diffusivity in following form, which has been used in this study:

$$K_{PX} = K_{PY} = K_H \frac{\sqrt{1 + (\frac{\beta w_t}{\sigma_{xy}})^2} - \frac{1}{2}\frac{\beta w_t}{\sigma_{xy}}}{1 + (\frac{\beta w_t}{\sigma_{xy}})^2} \tag{3.7.1}$$

$$K_{PZ} = K_Z \frac{1}{\sqrt{1 + (\frac{\beta w_t}{\sigma_Z})^2}} \tag{3.7.2}$$

where β is dimensionless coefficients, taken here to be 1, K_Z and K_H is horizontal and vertical eddy diffusivity of the air, σ_Z and σ_{xy} is the standard deviation of the turbulent velocity for vertical and horizontal direction, respectively, and w_t is the settling velocity of particle, which is estimated using (Lu and Shao, 2001)

$$w_t = \left(\frac{4\rho_p g D}{3\rho_{air} C_D} \right)^{1/2} \tag{3.7.3}$$

The horizontal and vertical standard deviation of the turbulent velocity was derived from surface-layer similarity relationship by Stull (1988).

$$\sigma_{XY} = \sqrt{\overline{u'^2}} = \sqrt{4.50 u_*^2} \tag{3.7.4}$$

$$\sigma_Z = \sqrt{\overline{w'^2}} = \sqrt{2.50 u_*^2} \tag{3.7.5}$$

3.8 Simulation Results

The considerable effort has been made to produce dust transport model, which can predict dust erosion patterns emitted from the exposed bottom of the Aral Sea and can adequately produce input data for the mortality rate evaluation model in the present research. The model was run for one year, during the period between January and December 2003, with the integration time step of 3 hours. It is not claimed that the model predictions perfectly accurate, and perfect erosion model has not been developed yet due to the existence of complex physical processes in the wind erosion. Given the difficulties involved in wind erosion prediction, the achievements of this study are obvious: the system correctly simulates wind erosion events in the Aral Sea and are in good agreement with visibility and timing features of one dust storm picture (Figure 3.1) taken from the satellite.

Over the one simulated year, the model was able to detect the number and transport direction of major dust storms event. It is found that the major transport direction, with frequency of 12,

was S, SSW, SW and WSW. The dust storm with the direction of E, ESE, SE, SSE was detected 6 times, and with N, NNE, NE, ENE direction 4 times. The strong W, WNW, NW and NNW ward dust storm events occurred only 2-3 times.

3.9 Validation with satellite image, episode of April 18, 2003

The simulated surface temperature, winds and streamlines fields are shown in Figure 3.1 and 3.3. The most outstanding feature of the flow fields was the strong northeasterly wind associated with a vigorous cool to cold airstreams for almost whole day. The location of frontal system can be easily identified from the narrow regions with sharp temperature gradients. It was found that wind erosion started in the early morning of 18 April, peaked at around 14:00 of the same day and eased at 18:00 of the same day. The simulated dust particle clouds, in general, show good agreement when compared with visibility features of the satellite picture. It should be recognized that the satellite images register only cases with very strong turbidity so in reality dust and salt could be transported to a far longer distance that can been seen from satellite picture. The shape, location and extend of the dust clouds coincide well with the wind erosion area predicted by model.

(a)

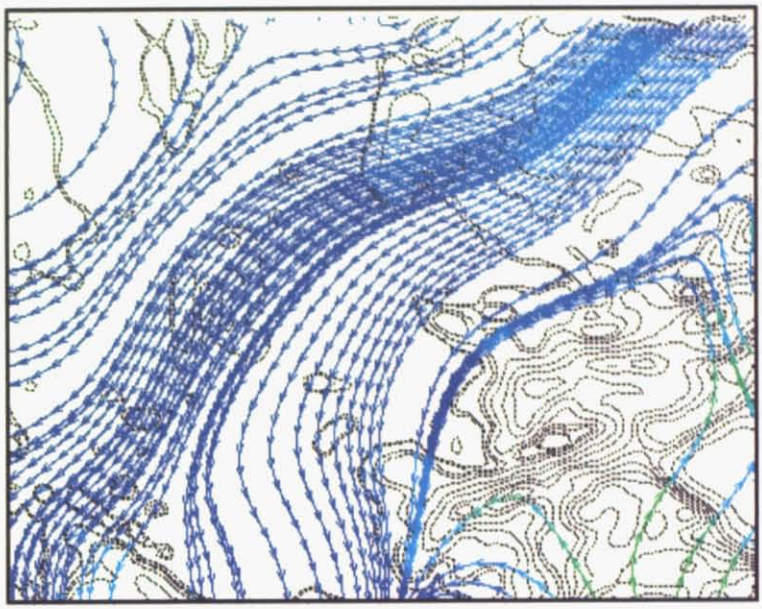

(b)

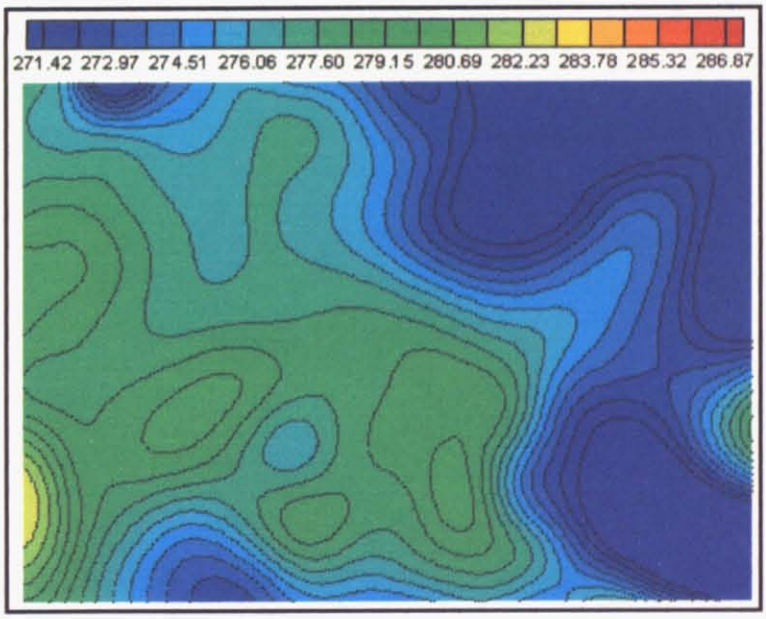

Figure 3.1 Simulated surface streamlines (a) and temperature (b)

for the 18 April, 2003 dust storm episode

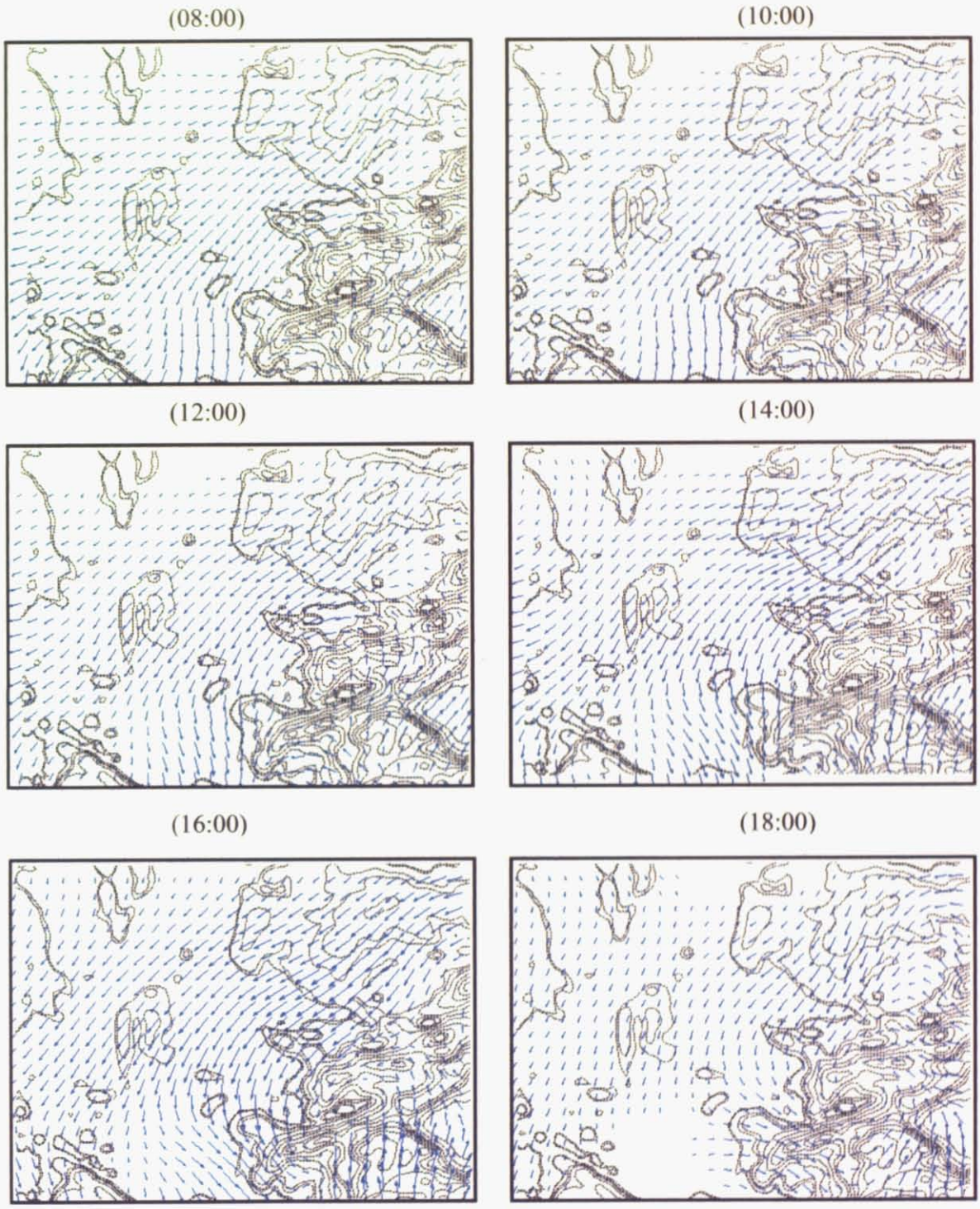

Figure 3.2 Wind field vectors for the 18 April, 2003 stormy day

(a)

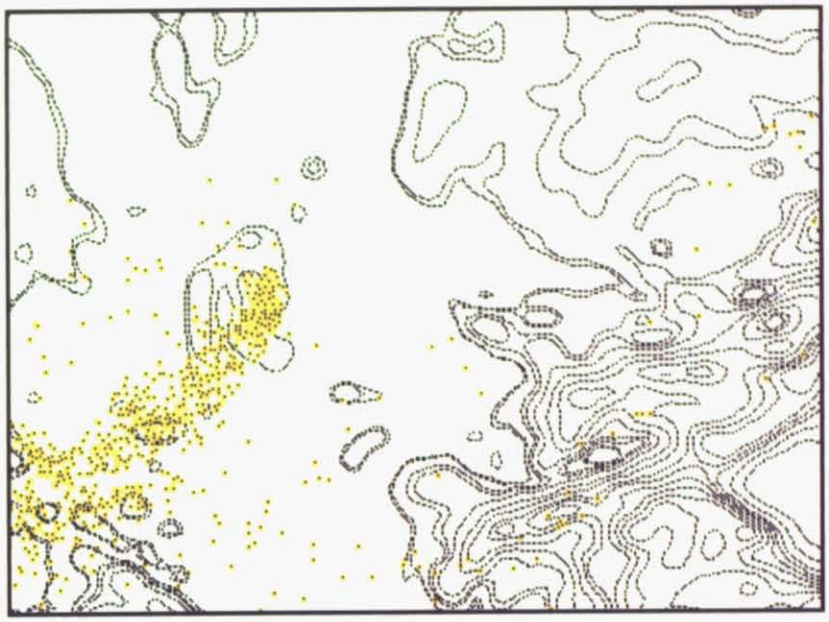

(b)

Figure 3.3 Observed (a) and simulated (b) of 18 April 2003 dust storm in the dried up seabed

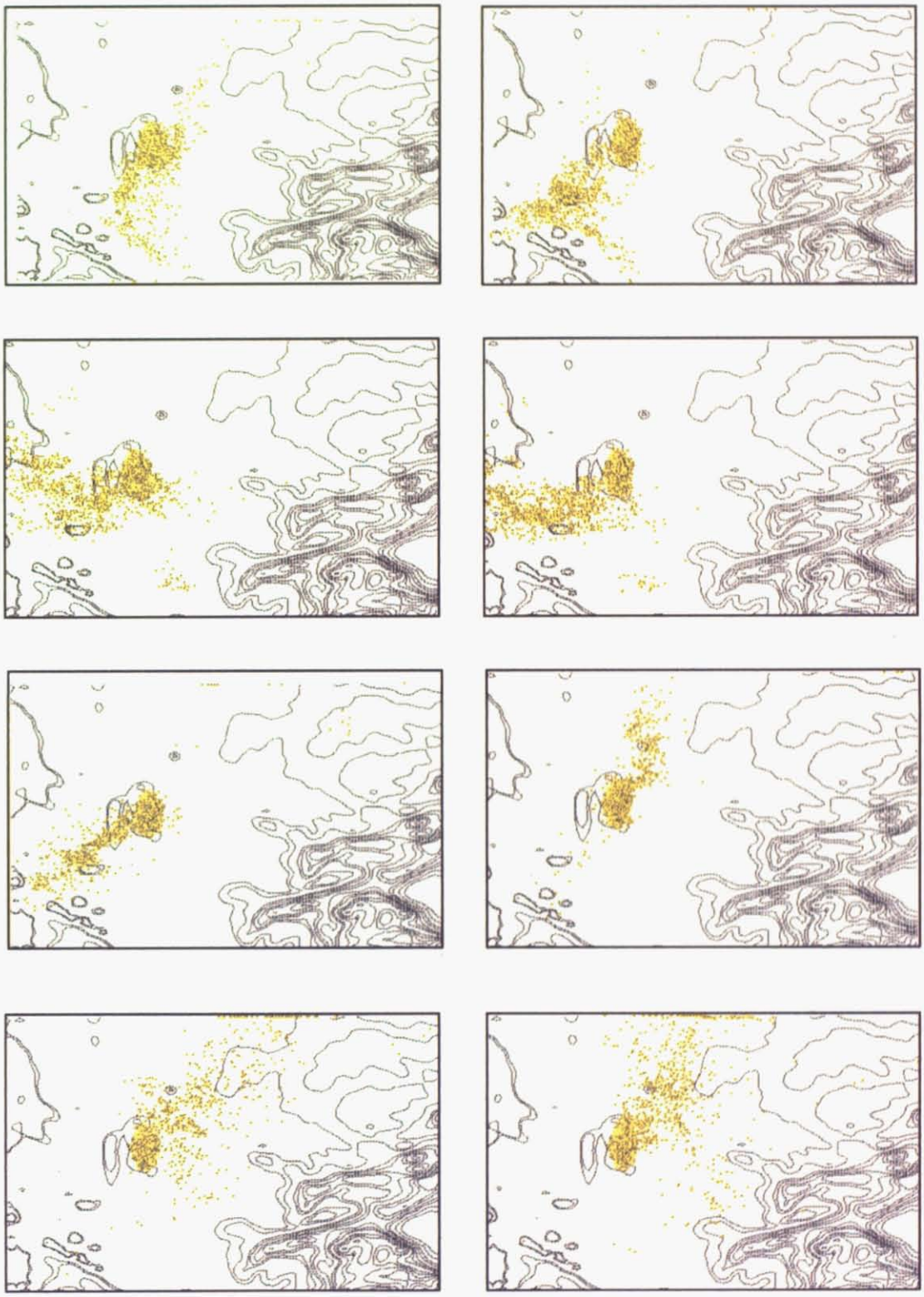

Figure 3.4 Major dust storm events in the former Aral Sea bed at various time and season

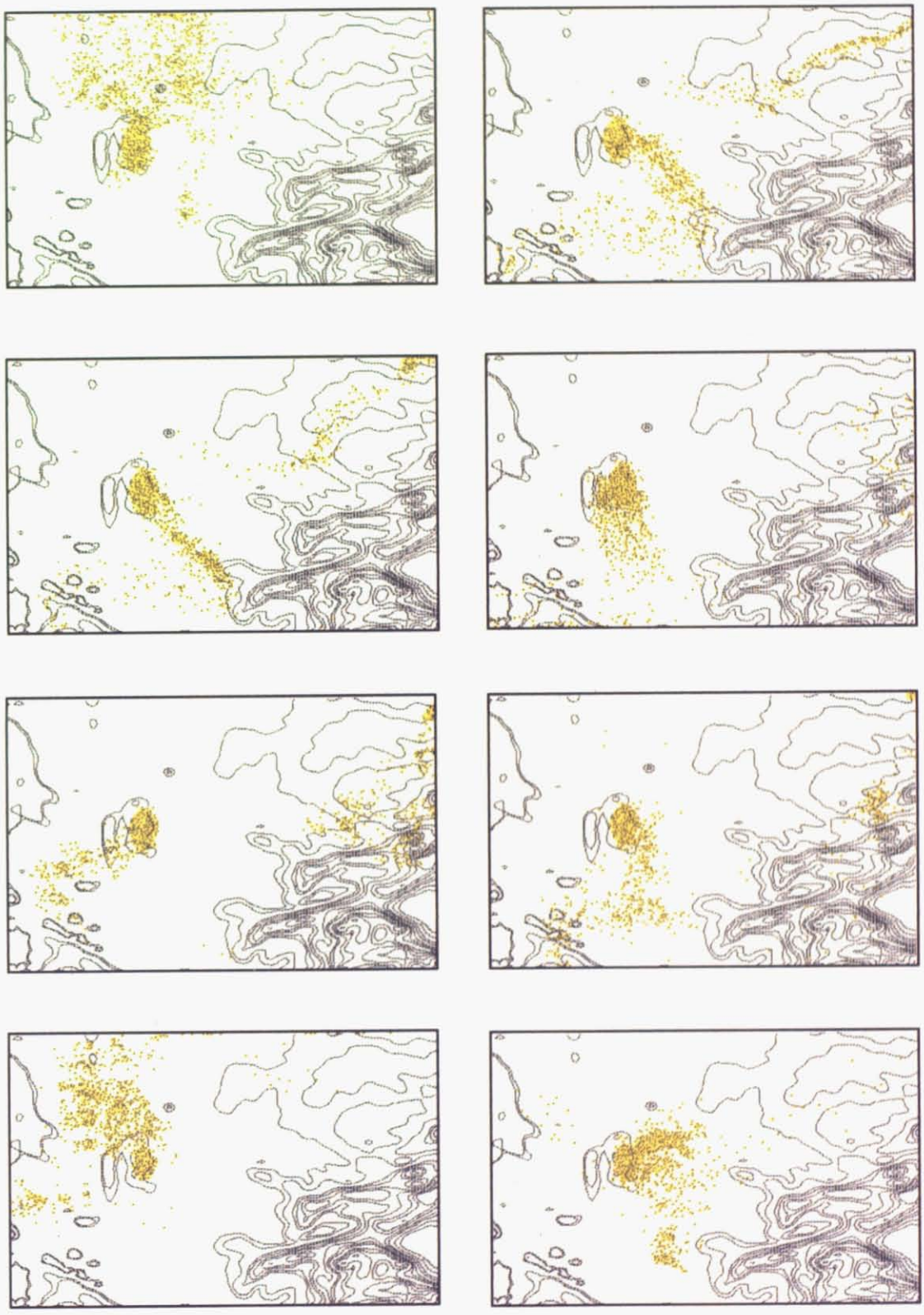

Figure 3.4 Major dust storm events in the former Aral Sea bed at various time and season

4. EFFECT OF DUST PARTICLES ON ANNUAL MORTALITY RATE

4.1 Overview

It is generally accepted that sever air pollution episodes, which are characterized by high level of dust particle pollution, have positive correlation with the increased mortality rate for cardiovascular and respiratory diseases. A significant number of reports and papers (Chen et al., 2003, Beer and Ricci, 1999, Dockery et al., 1992, Scarlet et al., 1995) have been published describing the particle concentration effect on the mortality of peoples. For instance, Deck et al. (1996) cited by Beer and Ricci (1999), found that $50\mu g / m^3$ increase of 1-day averaging in PM_{10}, leads to 2.5 % mortality increase.

Every year, windblown dust storms originating in the exposed bottom of the Aral Sea make their way to many highly populated cities in the region. These occurrences are known as White Dust Storm events among local population. The major effort in this chapter was given to describing the features of the model, which intended to evaluate the contribution of White Dust Storm on the annual standard mortality or death rate of the population living in Aral Sea basin, during the period of January and December 2003. Practical considerations are discussed, including the uncertainties introduced by demographic data gaps and modeling assumptions. The final output of the model is the numerical illustration of the contours of the regional mortality risk associated with windblown dust from the former Aral Sea seabed.

4.2 Definition of Dust

The particles in the atmosphere vary in size, composition and origin. It is often convenient to classify particles by their aerodynamic properties: (a) these properties govern the transport and removal of particles from the air; (b) they also govern their deposition within the respiratory system and (c) they are associated with the chemical composition and sources of particles. Because of its complexity and the importance of particle size in determining exposure and human dose, numerous terms are used to describe the dust particles. In the contents of human health study, particles are referred more to the site of deposition in the respiratory tract, e.g. "*inhalable particles*", which pass into the upper airways (nose and mouth), and "*thoracic particles*", which deposit within the lower respiratory tract, and "*respirable particles*", which penetrate to the gas-exchange region of the lung.

4.3 Annual Country Death Rate

The highlights on health provide an overview of the Central Asian Republics population death rate associated for all cases of death. As a rule, data have been taken for this purpose from one common international source: World Health Organization (WHO).

Table 4.1 Selected health indicators in Central Asian Republics and European Region

	Kazakhstan	Uzbekistan	Turkmenistan	Kyrgyzstan	Tajikistan
Standardized death rate for all causes of death per 100 000 population	1493.2	1236.2	1331.0	1336.7	1157.5

Source: World Health Organization

4.4 Methods

The distribution of dust concentrations are generated by Dust Transport model by combining area-specific population densities with atmospheric concentrations for each of the areas where contact to air pollutants occurs. The exposure-response function adopted from the reviewed literature. The change in mortality evaluated from the daily averaged particle matter concentrations in micrograms per cubic meter ($\mu g / m^3$) and gives quantitative measure of adverse effect of air pollution introduced by windblown dust emission from the dried bottom sea of the Aral Sea. The schematically explanation of the model is demonstrated in Figure 4.1.

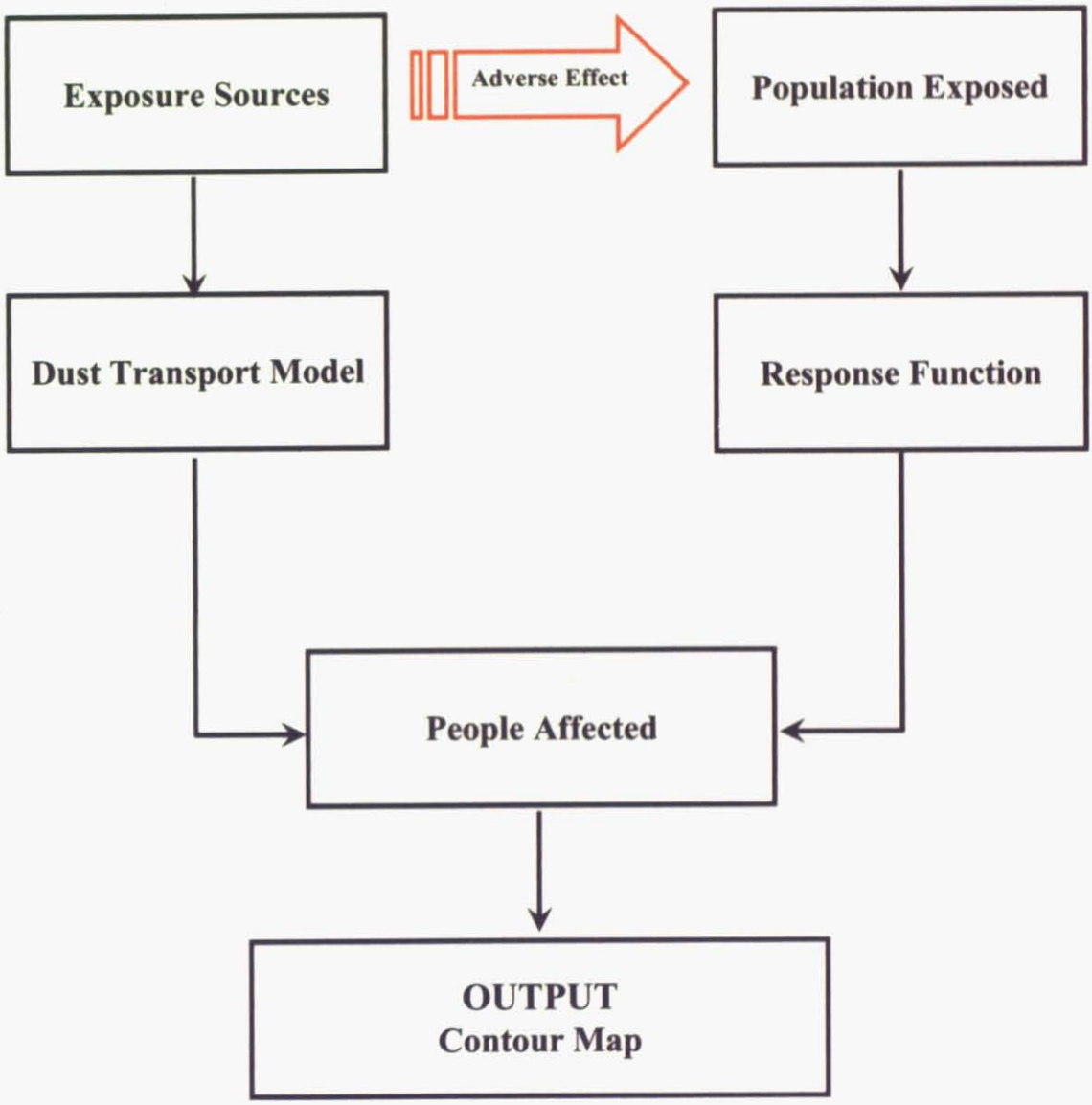

Figure 4.6 A block diagram of the model

4.5 Formulation of the response function in response to particle concentration

Deck et al. (1996) carried out a particle matter risk assessment for Philadelphia and Los Angeles. The concentration response functions used in their analysis were empirically estimated relationship between average ambient ambient concentrations of the pollutant of interest (PM) and the health endpoint of interest reported by epidemiological studies. Mathematically the relation given by

$$R(c) = r(o)\exp(\gamma c) = r(o)\,C_f \tag{4.4.1}$$

where $R(c)$ is the response function, c is the concentration of interest, thus here dust particle matter, C_f-change factor, $r(o)$ is a standard mortality rate used as endpoint, γ is given by

$$\gamma = \frac{\log_e(R_R)}{\Delta c} \tag{4.4.2}$$

where R_R represents relative risk for concentration change.

In this study, the same way as Deck et al. (1996) has been followed and used the relative risk (R_R) of 1.025 (a 2.5% increase) for mortality as a result of $\Delta c = 50\mu g/m^3$ increase in PM concentration, using one-day averaging time, so that $\gamma = 4.9\,\mathbf{x}\,10^{-4}$ was used.

Then the C_f factor response function be writing as follow

$$C_f = \exp(\gamma c) = R_R^{\frac{c}{\Delta c}} \tag{4.4.2}$$

By applying (4.4.2), the risk introduced by windblown particles from Aral Sea dried bottom at each grid point, per unit area, is obtained as

$$where\ RSK(c) = C_f(c) - 1 \tag{4.4.3}$$

where ρ_{PPL} expresses the density of population and $r(o)$ the death rate per unit of area.

However, at this point one should be noted that the $r(o)$, the death rate at each grid point is assumed same as country standard death rate for which the cell belongs to. Although knowing the fact that in practice, the mortality at each grid or the area differs considerably.

Finally, the annual death risk associated with Aral Sea, for each country, is defined as

$$RSK_C(c) = \frac{\int RSK(c) r(o) \rho_{PPL} dA}{\int \rho_{PPL} dA} \approx r(o) \frac{\int RSK(c) \rho_{PPL} dA}{\int \rho_{PPL} dA} \qquad (4.4.3)$$

where A is the total area of related country

4.6 Results from applying the method

The final result of this model is a function that expresses the actual number of people likely to be affected. Table 4.2 provides the final calculation of the model for 2003 year.

Table 4.2 Maximum values of population affected by dust particle concentration during the simulation period, 2003.

	Kazakhstan	Turkmenistan	Uzbekistan	Kyrgyzstan	Tajikistan
$\frac{\int RSK(c) \rho_{PPL} dA}{\int \rho_{PPL} dA}$	0.00062	0.00185	0.00396	0.00002	0.00001
$r(o)$	1493.2	1236.2	1331.0	1336.7	1157.5
$\int \rho_{PPL} dA$	15500000	4700000	24000000	4600000	6200000
Total People AFFECTED	143.4	107.5	1264.9	0.0	0.0

The Figure 4.7 demonstrates the numerical illustration of concentration response function. As expected, we observed that the Aral Sea dust storm has major impact on mortality rate of the population of Uzbekistan, Kazakhstan and Turkmenistan.

Results from this study identify high exposure areas for policy makers in a simple and realistic way, and can help generate hypothesis or show associations between population, health, and air quality indicators. In addition, the exposure assessments help provide some probabilistic estimates of the population likely to be affected. The mapping technique used can convey complex information very quickly and many people find the visual interpretation very easier than statistics information. Especially, for the case of Aral Sea problem, it helps the people to realize that most of the problem resulted from the wasteful water-consumption lifestyle. And since much of the blame is ours, we should have much obligation for finding solutions.

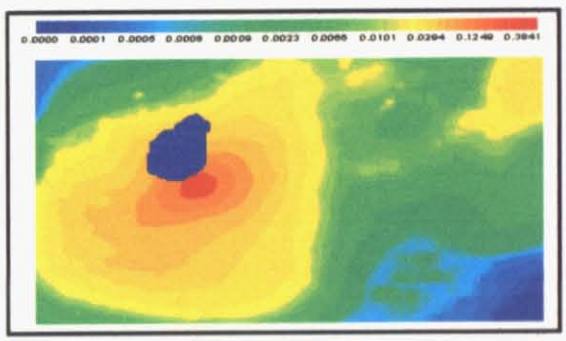

Figure 4.7 Contour map of concentration response function

Figure 4.8 Map of the region indicating the death rate associated with particle concentration windblown from the former Aral Sea bottom beautiful

5. CONCLUSION

The recession of the Aral Sea is as a result of excessive consumption of river inflow to the sea mainly for agriculture. To some critique, the problem of the Aral Sea is tied in with one main word, cotton. It is as a result of the cotton monoculture that excessive amount of water had to be diverted from the two feeder rivers (Amu Darya and Syr Darya) to the Aral Sea to supply irrigation plots. Added to this, damming of rivers and lakes for hydropower generation further worsened the situation as water was stored in reservoirs especially in countries up stream.

As a consequence, the Aral Sea has deteriorated into the largest inland body of salty reservoir in the world. Each year violent sandstorms pick up at least 500,000 tons of salt and sand from the dried-up seabed and transport it across hundreds of kilometres. The sands are contaminated with industrial and agricultural chemicals residue and have been linked to high

It is widely believed that this increased dust storm activity in the region has had a major impact on human health. Despite this fact, however, there is no comprehensive study on transfer of salts from the dried bottom of the sea, frequency, distribution and seasonality, estimation of its quantity and composition, the passes of transportation and those are the most important have not been investigated in great detail. Thus this research was considered to go some way towards bridging this gap.

To model the movement of dusts within the region to various vulnerable points at which it may directly be contacted by people, for this purpose an efficient computational model has been developed, in Chapter 2, to simulate an unsteady three-dimensional atmospheric flow over topography with the time and spatial resolution scales of the order of kilometers and of the order of minutes, respectively.

The Chapter 3 devoted to the description and formulation of transport and deposition modelling of sand and dust particles. The number of findings, dust storm patterns and its major pathways, detected by the model, compared with satellite image.

In Chapter 4 the major effort was given to describing the features of the model, which is used to evaluate the contribution of Dust Storm on the annual standard mortality or death rate of the population living in Aral Sea basin.

Over the one simulated, 2003, year, the model was able to detect the number and transport direction of major dust storms event. The simulated dust particle clouds show good agreement when compared with visibility features of the satellite picture. It was found that the major transport direction, with frequency of 12, was S, SSW, SW and WSW, which is associated with cyclonic intrusion from northeast triggered by the high-pressure system, forms over Siberia. The dust storm with the direction of E, ESE, SE, SSE was detected 6 times, and with N, NNE, NE, ENE direction 4 times. The strong W, WNW, NW and NNW ward dust storm events occurred only 2-3 times.

The most outstanding finding of the research is that the Aral Sea dust storm has major impact on mortality rate of the population of Kazakhstan, Turkmenistan and Uzbekistan. The number of people were affected by particle concentration in these countries, for 2003 year, have been approximated to be 143, 107 and 1264 respectively.

Finally, the mapping technique, which is used to visualize the results from this study, identifies high exposure areas for policy makers in a simple and realistic way, and can help generate hypothesis or show associations between population, health, and air quality indicators.

REFERENCE

1. Argaman E., Singer A. and Tsoar H., 2006. Erodibility of some crust forming soils/sediments from the Southern Aral Sea Basin as determined in a wind tunnel. Earth Surface Processes and Landforms, 31, 47-63.
2. Arnagel' dyev A.A. and Ivanov A.P., 1998. Breaking away and transport of sand particles by the wind. Problems of Desert Development, No. 2, pp. 43-47.
3. Beer T. and Ricci P.F., 1999. A quantitative risk assessment method based on population and exposure distribution using Australian air quality data. Env. Inter., Vol. 25, No. 6/7, pp. 887-898.
4. Beljaars A.C.M. and Holtslag A.A.M., 1990. Flux Parameterization over Land Surfaces for Atmospheric Models. J. of Appl. Mete., Vol. 30, pp. 327-341.
5. Berkowicz R. and Prahm L.P., 1982. Sensible Heat Flux Estimate from Routine Meteorological Data by the Resistance Method. J. of Appl. Mete., Vol. 21, pp.1845-1864.
6. Cahill T.A. and Parlange B.M., 1997. On the Brutsaert temperature roughness length model for sensible heat flux estimation. Water Resources Research, Vol. 33, No. 10, pp. 2315-2324.
7. Chen Y.S. and Yang C.Y., 2005. Effects of Asian dust storm events on daily hospital admissions for cardiovascular disease in Taipei, Taiwan. J., of Tox. and Env. Health, Part A, 68:1457-1464.
8. Chernyshev A.K., 1998. The use of space photographs to determine the transfer of salts from the dried up part of the Aral Sea. Problems of Desert Development, No. 3, pp. 59-62.
9. Chub V.E., 1998. Determining the influence of aerosols on the climatic characteristic of the Aral Sea Basin. Problems of Desert Development, No. 4, pp. 50-55.

10. Chub V.E., 1998. Investigation of Central Asian desert zones using satellite information. Problems of Desert development, No. 3, pp. 97-102.

11. Coulter R.L. and Martin T.J., 1996. Effects of Stability on the Profiles of Vertical Velocity and its Variance in Katabatic Flow. Boundary-Layer Meteorology 81, pp. 23-33.

12. Crighton J.E., Elliott J.S., Upshur R., van der Meer J. and Small I., 2003. The Aral Sea disaster and self-rated health. Health and Peace 9, pp. 73-82.

13. Deck L., Post E., Wiener M. and Dunningham K., 1995. A particle matter risk assessment for Philadelphia and Los Angeles. Report to USEPA. Cambridge, MA: Abt Associates, 1996.

14. Denisov Yu.M., 1998. The formation and transfer of aerosols. Problems of Desert Development, No. 3, pp. 21-25.

15. Esenov P., 1998. Salt migration processes in the Turkmenistan part of the CIS-Aral area. Problems of Desert Development, No. 4, pp. 70-75.

16. Galaeva O.S., 1998. Monitoring of the removal of a sand and salt aerosol from the dried up part of the Aral Sea. Problems of Desert Development, No. 4, pp. 17-21.

17. Galaeva, O. S. and Semenov O. E., 1997. On monitoring of the blowout of the sandy salty aerosol from the dried bottom of the Aral Sea. Hydrometeorology and ecology, 2 (in Russian).

18. Genthon C., 1992. Simulation of desert dust and sea-salt aerosols in Antarctica with a general circulation model of the atmosphere.

19. Ivanov Y.N., Chub V.E., Subbotina O.I., Tolkacheva G.A. and Toryannikova R.V., 1996. Reviews of the scientific and environmental issues of the Aral Sea basin. The Aral Sea Basin, NATO ASI Series, Partnership Sub-Series, 2. Env.-Vol.12.

20. Jiang D., Liu H. and Wang W., 2001. Test a modified surface wind interpolation scheme for complex terrain in a stable atmosphere. Atm. Env. 35, pp. 4877-4885.

21. Kamalov S., 1998. Processes of salt migration in Karakalpakstan. Problems of Desert Development, No. 3, pp. 25-35.

22. Montero G., Montenegro R. and Escobar J.M., 1998. A 3-D diagnostic model for wind field adjustment. J.Win.Eng.&Ind.Aer. 74-76, 249-261.

23. Kamalov S.K., 1996. Climatic and ecological effects of the environmental changes in the Aral Sea zone on Karakalpakstan. The Aral Sea Basin, NATO ASI Series, Partnership Sub-Series, 2. Env.-Vol.12

24. Kurbaniyazov A.K., 1998. Relief-forming processes on the dried-up Aral Sea bottom. Problems of Desert Development, No. 2, pp. 83-85.

25. Kurbatkin V.P. and Filippov S.G., 1998. Ways of controlling salt transfer. Problems of Desert Development, No. 4, pp. 45-50.

26. Liu Y.C. and Goodin R.W., 1975. An Iterative Algorithm for Objective Wind Field Analysis. Monthly Weather Review, Vol. 104, pp. 784-792.

27. Lu H. and Shao Y., 2001. Toward quantitative prediction of dust storms: an integrated wind erosion modeling system and its applications. Env. Mod.&Soft., 16, 233-249.

28. Mohan M. and Siddiqui T.A., 1998. Analysis of various schemes for the estimation of atmospheric stability classification. Atm. Env., Vol. 32, No. 21, pp. 3775-3781.

29. Narayana Rao D., Ratnam M.V., Rao T.N. and Rao S.V.B., 2001. Seasonal variation of vertical eddy diffusivity in the troposphere, lower stratosphere and mesosphere over a tropical station. Annales Geophysicae 19: 975-984.

30. Nasonov V.G. and Ruziev I.B., 1998. Influences of salt migration on the state of the irrigated lands in the Aral Sea Basin. Problems of Desert Development, No. 4, pp. 75-81.

31. Nickerson C.E. and Smiley E.V., 1974. Surface Layer and Energy Budget Parameterizations for Mesoscale Models. J. of Appl. Mete., Vol. 14, pp. 297-300.

32. Nieuwstadt F., 1977. The computation of the friction velocity and the temperature scale *T* from temperature and wind velocity profiles by least-square methods. Boundary-Layer Meteorology 14, pp. 235-246.

33. Ogurtsov V.Y., 1998. Laws of the change in the transparency of the ties shan atmosphere.

Problems of Desert Development, No. 4, pp. 87-96.

34. Paulson A.C., 1970. The Mathematical Representation of Wind Speed and Temperature Profiles in the Unstable Atmospheric Surface Layer. J. of Appl. Mete., Vol. 9, pp.857-861.
35. Popov V.A., 1998. The role of salt migration in landscape genesis of the CIS-Aral region. Problems of Desert Development, No. 3, pp. 122-126.
36. Ptichnikov A., 1996. Environmental and landscape changes in the Aral Sea region as detected from remote sensing. The Aral Sea Basin, NATO ASI Series, Partnership Sub-Series, 2. Env.-Vol.12.
37. Gillette D. A., Niemeyer T. C. and Helm P. J., 2001.Supply-limited horizontal sand drift at an ephemerally crusted, unvegetated saline playa, J. Geophys. Res., 106(D16), 18085-18098, 10.1029/2000JD900324.
38. Stewart O. G. and Gillette D. A., 2001. Distribution of vegetation in wind-dominated landscapes: Implications for wind erosion modeling and landscape processes, J. Geophys. Res., 106(D9), 9673-9684, 10.1029/2001JD900052.
39. Gillette D. A., Marticorena B. and Bergametti G., 1999. Change in the aerodynamic roughness height by saltating grains: Experimental assessment, test of theory, and operational parameterization, J. Geophys. Res., 103(D6), 6203-6210, 10.1029/98JD00207.
40. Gillette D. A., Fryrear D. W., Gill T. E., Ley T., Cahill T. A. and Gearhart E. A., 1997. Relation of vertical flux of particles smaller than 10 &mgr;m to total aeolian horizontal mass flux at Owens Lake, J. Geophys. Res., 102(D22), 26009-26016, 10.1029/97JD02252.
41. Marticorena B., Bergametti G., Gillette D. and Belnap J., 1997. Factors controlling threshold friction velocity in semiarid and arid areas of the United States, J. Geophys. Res., 102(D19), 23277-23288, 10.1029/97JD01303.
42. Gillette D. A., Hardebeck E. and Parker J., 1997. Large-scale variability of wind erosion mass flux rates at Owens Lake. 2. Role of roughness change, particle limitation, change of

threshold friction velocity, and the Owen effect, J. Geophys. Res., 102(D22), 25989-25998, 10.1029/97JD00960.

43. Gillette, D. A., Fryrear D. W., Xiao J. B., Stockton P., Ono D., Helm P. J., Gill T. E. and Ley T., 1997. Large-scale variability of wind erosion mass flux rates at Owens Lake. 1. Vertical profiles of horizontal mass fluxes of wind-eroded particles with diameter greater than 50 &mgr;m, J. Geophys. Res., 102(D22), 25977-25988, 10.1029/97JD00961.
44. Raupach, M. R., Gillette D. A. and Leys J. F., 1993. The effect of roughness elements on wind erosion threshold, J. Geophys. Res., 98(D2), 3023-3029, 10.1029/92JD01922.
45. Gillette, D. A., Hanson K. J, 1989. Spatial and temporal variability of dust production caused by wind erosion in the United States, J. Geophys. Res., 94(D2), 2197-2206, 10.1029/88JD03917.
46. Gillette, D. A. and Stockton P. H., 1989. The effect of non-erodible particles on wind erosion of erodible surfaces, J. Geophys. Res., 94(D10), 12885-12893, 10.1029/89JD00758.
47. Gillette, D. A. and Passi R., 1988. Modeling dust emission caused by wind erosion, J. Geophys. Res., 93(D11), 14233-14242, 10.1029/88JD03082.
48. Gillette D., Ono D. and Richmond K., 2004. A combined modeling and measurement technique for estimating windblown dust emissions at Owens (dry) Lake, California, J. Geophys. Res., 109, F01003, doi:10.1029/2003JF000025.
49. Press W.H., Flannery B.P., Teukolsky A.S. and Vetterling T.W. 1986. Numerical Recipes. The art of scientific computing. Cambridge Uni.Press.
50. Rainer R., 1996. Monitoring of recent area and volume changes of the Aral Sea and development of an optimized land and water use model for the Amu Dar'ya delta. The Aral Sea Basin, NATO ASI Series, Partnership Sub-Series, 2. Env.-Vol.12
51. Razakov R.M. and Kosnazarov K.A., 1996. Dust and salt transfer from the exposed bed of the Aral Sea and measures to decrease its environmental impact. The Aral Sea Basin,

NATO ASI Series, Partnership Sub-Series, 2. Env.-Vol.12

52. Razakov R.M. and Kosnazarov K.A., 1998. Migration of salts and toxicants in the CIS-Aral region. Problems of Desert Development, No. 4, pp. 63-70.
53. Roger A. and Pielke S.R., 1984. Mesoscale Meteorological Modeling. Academic Press, California.
54. Ross D.G., Smith I.N., Manins P.C. and Fox D.G., 1988. Diagnostic Wind Field Monitoring for Complex Terrain: Model Development and Testing. J. of Appl. Mete., Vol. 27, pp. 785-796.
55. Rubanov I.V., Pinkhasov E.I. and Kurbaniyazov A.K., 1998. Process of salt accumulation in the Aral Sea. Problems of Desert Development, No. 4, pp. 31-36.
56. Satyanarayana A.N.V., Lykossov V.N., Mohanty U.C. and Machul'skaya E.E., 2002. Parameterization of Land Surface Processes to Study Boundary Layer Characteristics over a Semiarid Region in Northwest India. J. of Appl. Mete., Vol. 42, pp. 528-540.
57. Semenov O.E., 1998. Precipitation of a sand and salt aerosol onto the surface of the CIS-Aral region. Problems of Desert Development, No. 3, pp. 37-44.
58. Sergeev A.I., 1998. A method of calculating the evacuation of salts and contamination from irrigated lands. Problems of Desert Development, No. 3, pp. 81-87.
59. Shao Y. and Leslie L.M., 1997. Wind erosion prediction over the Australian continent. J. of Geo.Res., Vol.102. D25, pp.30,091-30,105.
60. Shao Y., 2000. Physics and Modeling of Wind Erosion. London, Kluwer.
61. Singer A., Zobeck T., Poberezsky L. and Argaman E., 2003. The PM_{10} and $PM_{2.5}$ dust generation potential of soils/sediments in the Southern Aral Sea Basin, Uzbekistan. J. of Arid Env. 54: 705-728.
62. Small E.E., Sloan C.L. and Nychka D., 2000. Changes in Surface Air Temperature Caused by Desiccation of the Aral Sea. J. of Climate, Vol. 14.
63. Song Z., 2004. A numerical simulation of dust storm in China. Env.Mod.&Soft. 19,

141-151.

64. Stearns R.C., 1969. Determining Surface Roughness and Displacement Height. Boundary-Layer Meteorology 1, pp. 102-111.

65. Stulina G. and Sektimenko V., 2003. The changes in soil cover on the exposed bed of the Aral Sea. J. of Marine Systems 47, pp. 121-125.

66. Stull R.B., 1988. An Introduction to Boundary Layer Meteorology. London, Kluwer.

67. Sun J., Zhao L., Zhao S. and Zhang R., 2006. An integrated dust storm prediction system suitable for East Asia and its simulation results. Global and Planetary Change 52, pp. 71-87.

68. Tolkacheva G.A., Kovalevskaya Yu.I. and Shardakova L.Yu., 1998. Determination of salt migration in the Aral Sea Basin. Problems of Desert Development, No. 3, pp. 55-59.

69. van Dop H., 1983. Terrain classification and derived meteorological parameters for interregional transport models. Atm. Env., Vol. 17, No. 6, pp. 1099-1105.

70. van Ulden A.P. and Holtslag A.A.M., 1985. Estimation of Atmospheric Boundary Layer Parameters for Diffusion Applications. J. of Climate and Appl. Mete., Vol. 24, pp. 1196-1207.

71. Wiggs S.G., O'hara S., Wegerdt J., van de Meer J., Small I. and Hubbard R., 2003. The dynamics and characteristics of Aeolian dust in dryland Central Asia: possible impacts on human exposure and respiratory health in the Aral Sea basin. The Geographical J., Vol. 169, No. 2, pp. 142-157.

72. Yang K., Huang G. and Tamai N., 2000. Improvement of surface process for application of a NWP system. Annual J. of Hydraulic Engineering, JSCE, Vol. 44, pp. 61-66.

73. Yang K., Koike T., Fujii H., Tamagawa K. and Hirose N., 2002. Improvement of surface flux parameterizations with a turbulence-related length. Q.J.R. Meteorol. Soc. 128, pp. 2073-2087.

74. Yang K., Tamai N. and Koike T., 2001. Analytical Solution of Surface Layer Similarity

Equations. J. of Appl. Mete., Vol. 40, pp. 1647-1653.

75. Zhang D.L. and Fritsch M.J., 1988. A Numerical Investigation of a Convectively Generated, Inertially Stable, Extratropical Warm-Core Mesovortex over Land. Part I: Structure and Evolution. Monthly Weather Review, Vol. 116, pp. 2660-2669.
76. Zilitinkevich S.S., 1972. On the determination of the height of the Ekman boundary layer. Boundary-Layer Meteorology 3, pp. 141-145.
77. Zilitinkevich S.S., 1988. Velocity Profiles, the Resistance Law and the Dissipation Rate of Mean Flow Kinetic Energy in a Neutrally and Stably Stratified Planetary Boundary Layer. Boundary-Layer Meteorology 46, pp. 367-387.
78. Zobeck T.M., Popham T.W., Skidmore E.L., Lamb J.A., Merrill S.D., Lindstrom M.J., Mokma D.L. and Yoder R.E., 2003. Aggregate-Mean Diameter and Wind-Erodible Soil Predictions Using Dry Aggregate-Size Distributions. Soil Sci. Soc. Am. J. 67: 425-436.

NUMERICAL SIMULATION AND POPULATION-WIDE RISK ASSESSMENT OF WINDBLOWN DUST EMISSION FROM DRIED-UP BOTTOM OF ARAL SEA

Bakhtiyor NAKHSHINIEV
Supervisor prof. Toru SATO

1.INTRODUCTION

The Aral Sea, once one of the world's largest inland seas, is now shrinking due to unsustainable water consumption from its inflow rivers by the Central Asian Republics (the culprit. As a consequence of the increased of irrigated area and hydropower generation in the Aral Sea basin, coupled with population increase, the Aral Sea has deteriorated into the largest inland body of salty reservoir in the world. The Aral Sea case is a very prime example of how unsustainable action can lead to an environmental disaster. The process of degradation of the Aral Sea did not only posed environmental consequences but alongside, severe social and economic crises. Each year violent sandstorms pick up at least 150,000 tons of salt and sand from the dried-up seabed and transport it across hundreds of kilometres. The sands are contaminated with industrial and agricultural chemicals residue and have been linked to high regional rates of respiratory diseases and certain types of cancer. A depressed fact is that the primary victims of these crises are the most vulnerable strata of the region's society, wiz children, elderly peoples with pre-existing asthmatic illness, women and less-paid inhabitants of cities and rural areas. The main objective of this research is a simulation of dust particle transport from the exposed bottom of the Aral Sea and evaluation of annual mortality rate introduced by windblown dust emission from dried bottom of Aral Sea.

Study follows an integrated approach and conceptually consists of two models: 1) numerical simulation of dust concentrations blown from the dried-up bottom of Aral Sea and 2) population-wide assessment model, which reads dust concentrations data from simulation model. Therefore, to model the movement of dusts within the region to various vulnerable points at which it may be contacted by people, a wind flow field has been developed.

2. DEVELOPMENT OF WIND FLOW MODEL

2.1 Wind field computations process

Initially, the wind filed was obtained in two steps. First, the values of Surface Friction-u_*, Air Temperature-T, Surface Pressure-P, Sensible Heat Flux-Q, Roughness Height-z_0 and Geopotential Height-Z_{GP} were approximated in the points of the domain located at the same height z_0 over the terrain using a *horizontal bi-cubic spline interpolation*. Then from this information we perform a *vertical extrapolation* to define the velocity filed in the whole domain. To find the fields at desired time, temporary interpolation was also carried out.

2.2 Vertical extrapolation

In this study, a log-linear wind profile is considered in vertical direction. This takes into account the horizontally interpolated variables and the effect of roughness on the wind intensity and direction (Montero, 1998). Above the surface layer (Z_{sl}), a linear interpolation is made using the geostrophic wind. The logarithmic profile of wind in vertical direction is given by

$$u(z) = \frac{u_*}{k}\left(\log\frac{z}{z_0} - \psi_m\left(\frac{z}{L}\right)\right). \qquad (2.1)$$

where u_* is friction velocity, k-is Von-Karman constant, z_0- is the roughness height and Z_{sl} is the height of the surface layer. The value ψ depends on the air stability and obtained by following equations (Stull,1988).

For neutral atmosphere, ,

$$\psi\left(\frac{z}{L}\right) = 0, \qquad (2.2)$$

for stable atmosphere, ,

$$\psi\left(\frac{z}{L}\right) = -5 * \frac{z}{L}, \qquad (2.3)$$

and finally for unstable atmosphere,

$$\psi\left(\frac{z}{L}\right) = \log\left[\left(\frac{x^2+1}{2}\right)\left(\frac{x+1}{2}\right)^2\right] - 2\arctan x + \frac{\pi}{2} \quad (2.4)$$

where, $x = (1-16z/L)^{1/4}$ and L is Obukhov

2.3 Vertical wind velocity.

The vertical wind velocity is not an observed variable, and yet, its estimation appears as one of the most difficult problem for the meteorologists. However, if the wind observation is available on a grid array, the estimation of kinematic vertical velocity can obtained straightforwardly from the integration of the mass continuity equation.

The equation of continuity is:

$$\frac{\partial u}{\partial x} + \frac{\partial v}{\partial y} + \frac{\partial w}{\partial z} = 0 \quad (2.3.1)$$

Under this strong constrain of mass conservation the vertical motion is obtained by:

$$w(z) = -\int_0^z \left(\frac{\partial u}{\partial x} + \frac{\partial v}{\partial y}\right) dz. \quad (2.3.2)$$

3. MODELLING OF DUST TRANSPORT

The transport scheme predicts the dust concentration by solving the following system of equation in Lagrangian framework:

$$\left(m_p + \frac{\rho_f V_p}{2}\right)\frac{d\mathbf{u}_p}{dt} = -V_p \nabla P + m_p \mathbf{g} - \frac{1}{2}\rho_f S C_D \mathbf{u}_r |\mathbf{u}_r| \quad (3.1)$$

$$\frac{d\mathbf{x}_p}{dt} = \mathbf{u}_p \quad (3.2)$$

Here $\mathbf{x}_p$ is the particle position, m_p is the particle mass, ρ is the fluid (air) density, V_p is the volume of particle, $\mathbf{u}_p$ is the particle velocity, ∇P is the pressure gradient, $\mathbf{g}$ is gravity, S is the cross-section of the particle in $\mathbf{u}_r$ direction, C_D is the drag coefficient, $\mathbf{u}_r$ is particle-to-fluid relative velocity, which is defined by

$$\mathbf{u}_r = \mathbf{u}_p - \mathbf{u} \quad (3.3)$$

The value of $\mathbf{u}$ is determined by interpolating fluid velocity from grid point to the location of particle.

The effect of the subgrid turbulent fluctuations of air motion are also need to be considered in the calculation of particle motion, therefore, x_p is expressed as

$$\mathbf{x}_p^{n+1} = \mathbf{x}_p^n + \Delta t \mathbf{u}_p + \sqrt{2K_p \Delta t}\,\chi \quad (3.4)$$

where the last term in the equation represents a simple dispersion of particles, adopted from Suzuki (2001). K_p, here, expresses particle eddy diffusivity and χ represents the Gaussian probability distribution function. The numerical solution of this function described in Press et al. (1992).

The magnitude of the aerodynamic drag depends on the flow patters around the particle. The $C_D(Re_p)$ relationship has been approximately determined by using Morci and Alexaner (1972) functions

$$C_D(Re_p) = \frac{k_1}{Re_p} + \frac{k_2}{Re_p} + k_3 \quad (3.4)$$

The particle Reynolds number defined as

$$Re_p = \frac{|\mathbf{u}_p - \mathbf{u}| D_p}{\nu_{air}} \quad (3.5)$$

where ν_{air} air viscosity and D_p is particle diameter.

3.1 Validation with satellite image

The simulated surface temperature, winds and streamlines fields are shown in Figure 3.1 and 3.3. The most outstanding feature of the flow fields was the strong northeasterly wind associated with a vigorous cool to cold airstreams for almost whole day. The location of frontal system can be easily identified from the narrow regions with sharp temperature gradients. It was found that wind erosion started in the early morning of 18 April, peaked at around 14:00 of the same day and eased at 18:00 of the same day. The

simulated dust particle clouds, in general, show good agreement when compared with visibility features of the satellite picture. It should be recognized that the satellite images register only cases with very strong turbidity so in reality dust and salt could be transported to a far longer distance that can seen from satellite picture. The shape, location and extend of the dust clouds coincide well with the wind erosion area predicted by model.

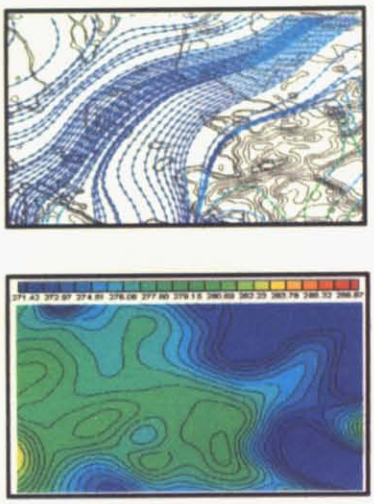

Figure 3.1 Simulated surface streamlines (a) and temperature (b) for the 18 April, 2003

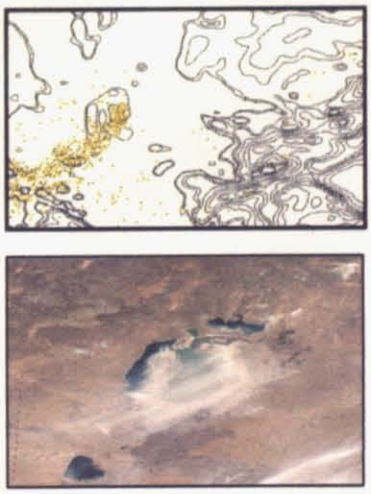

Figure 3.3 Observed (a) and simulated (b) of 18 April 2003 dust storm in the dried up seabed

4. EFFECT OF DUST PARTICLES ON ANNUAL MORTALITY RATE

4.1 Methods

The distribution of dust concentrations are generated by Dust Transport model by combining area-specific population densities with atmospheric concentrations for each of the areas where contact to air pollutants occurs. The exposure-response function adopted from the reviewed literature. The change in mortality evaluated from the daily averaged particle matter concentrations in micrograms per cubic meter and gives quantitative measure of adverse effect of air pollution introduced by windblown dust emission from the dried bottom sea of the Aral Sea.

4.2 Formulation of the response function in response to particle concentration

Deck et al. (1996) carried out a particle matter risk assessment for Philadelphia and Los Angeles. The concentration response functions used in their analysis were empirically estimated relationship between average ambient ambient concentrations of the pollutant of interest (PM) and the health endpoint of interest reported by epidemiological studies. Mathematically the relation given by

$$R(c) = r(o)\exp(\gamma c) \quad (4.2.1)$$

where $R(c)$ is the response function, c is the concentration of interest, thus here dust particle matter, $r(o)$ is a standard mortality rate used as endpoint, γ is given by

$$\gamma = \frac{\log_e(RR)}{\Delta c} \quad (4.2.2)$$

where RR represents relative risk for concentration change.

In this study, the same way as Deck et al. (1996) has been followed and used the relative risk *(RR)* of 1.025 (a 2.5% increase) for mortality as a result of

$\Delta c = 50 \mu g / m^3$ increase in PM concentration, using one-day averaging time, so that $\gamma = 4.9 \mathbf{x} 10^{-4}$ was used. Then the concentration response function be writing as follow

$$R(c) = r(o) \exp(4.9 \mathbf{x} 10^{-4} c) \quad (4.2.3)$$

However, to avoid the computational problem, which may be often caused by large value of c, after small side calculation we rewrite (4.4.2) in more suitable form

$$R(c) = 1.025^{\frac{c}{\Delta c}} r(o)$$

4.3 Results from applying the method

The final result of this model is a function that expresses the actual number of people likely to be affected.

(a)

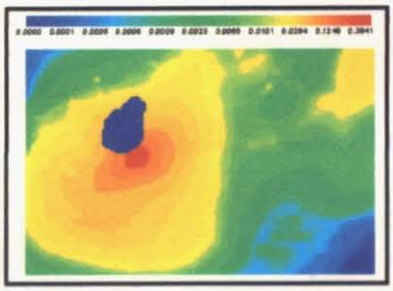

(b)

Figure 4.7 Contour map of concentration response function: (a) on each cell, (b) averaged for each republics

The Figure 4.7 demonstrates the numerical illustration of concentration response function. As expected, we observed that the Aral Sea dust storm has major impact on mortality rate of the population of Uzbekistan, Kazakhstan and Turkmenistan.

Results from this study identify high exposure areas for policy makers in a simple and realistic way, and can help generate hypothesis or show associations between population, health, and air quality indicators. In addition, the exposure assessments help provide some probabilistic estimates of the population likely to be affected. The mapping technique used can convey complex information very quickly and many people find the visual interpretation very easier than statistics information. Especially, for the case of Aral Sea problem, it helps the people to realize that most of the problem resulted from the wasteful water-consumption lifestyle. And since much of the blame is ours, we should have much obligation for finding solutions.

REFERENCES

1. Montero G., Montenegro R. and Escobar J.M., 1998. A 3-D diagnostic model for wind field adjustment. J.Win.Eng.&Ind.Aer. 74-76, 249-261.
2. Stull R.B., 1988. An Introduction to Boundary Layer Meteorology. London, Kluwer.
3. Deck L., Post E., Wiener M. and Dunningham K., 1995. A particle matter risk assessment for Philadelphia and Los Angeles. Report to USEPA. Cambridge, MA: Abt Associates.
4. Suzuki T., 2001. Numerical Simulation of Scalar Fluctuation Filed in a Non-Buoyant Plume by Random fourier Modes. Trans. of JSCES, No.200010004